Running Title: Immunity-and-Matrix-Regulatory Cells Derived from hESCs…

Immunity-and-Matrix-Regulatory Cells Derived from Human Embryonic Stem Cells Safely and Effectively Treat Mouse Lung Injury and Fibrosis

Jun Wu[1,2,3,16], Dingyun Song[6,7,16], Zhongwen Li[1,2,3,16], Baojie Guo[1,2,3,4,16], Yani Xiao[11], Wenjing Liu[1,2,3], Lingmin Liang[1,2,3], Chunjing Feng[1], Tingting Gao[1,2,3], Yanxia Chen[1,2,3], Ying Li[15], Zai Wang[8], Jianyan Wen[8,9], Shengnan Yang[6,10], Peipei Liu[6,7], Lei Wang[1,2,3], Yukai Wang[1,2,3], Liang Peng[8], Glyn Nigel Stacey[3,5], Zheng Hu[13,14], Guihai Feng[1,2], Wei Li[1,2], Yan Huo[11], Ronghua Jin[12], Ng Shyh-Chang[1,2,4], Qi Zhou[1,2,3,4], Liu Wang[1,2,3,4,*], Baoyang Hu[1,2,3,4,*], Huaping Dai[6,7,*] and Jie Hao[1,2,3,*]

[1] State Key Laboratory of Stem Cell and Reproductive Biology, Institute of Zoology, Chinese Academy of Sciences, Beijing 100101, China

[2] Institute for Stem Cell and Regeneration, Chinese Academy of Sciences, Beijing 100101, China

[3] National Stem Cell Resource Center, Chinese Academy of Sciences, Beijing 100101, China

[4] University of Chinese Academy of Sciences, Beijing 100049, China

[5] International Stem Cell Banking Initiative, Hertfordshire, UK

[6] Department of Pulmonary and Critical Care Medicine, Center of Respiratory Medicine, China-Japan Friendship Hospital; National Clinical Research Center for Respiratory Diseases, Institute of Respiratory Medicine, Chinese Academy of Medical Sciences; Beijing 100029, China

[7] Graduate School of Peking Union Medical College, Chinese Academy of Medical Science and Peking Union Medical College, Beijing 100730, China

[8] Institute of Clinical Medical Sciences, Center of Respiratory Medicine, China-Japan Friendship Hospital, Beijing, China; Institute of Respiratory Medicine, Chinese Academy of Medical

Sciences, Beijing, China

[9] Department of Cardiology, China-Japan Friendship Hospital; Beijing 100029, China

[10] Medical University of Ha Er Bin, Heilong Jiang Province, China

[11] National Center for Safety Evaluation of Drugs, National Institutes for Food and Drug Control, Beijing 100176, China

[12] Beijing Youan Hospital, Capital Medical University

[13] Key Laboratory of Organ Regeneration & Transplantation of Ministry of Education, The First Hospital of Jilin University, Changchun 130061, China

[14] National-Local Joint Engineering Laboratory of Animal Models for Human Diseases, Changchun 130061, China

[15] Department of Gastroenterology, The First Hospital of Jilin University, Changchun, 130061, China

[16] These authors contributed equally.

*Correspondence: haojie@ioz.ac.cn, byhu@ioz.ac.cn, daihuaping@ccmu.edu.cn, wangliu@ioz.ac.cn

Abstract

Lung injury and fibrosis represent the most significant outcomes of severe and acute lung disorders, including COVID-19. However, there are still no effective drugs to treat lung injury and fibrosis. In this study, we report the generation of clinical-grade human embryonic stem cells (hESCs)-derived immunity- and matrix-regulatory cells (IMRCs) produced under good manufacturing practice (GMP) requirements, that can treat lung injury and fibrosis in vivo. We generate IMRCs by sequentially differentiating hESCs with xeno-free reagents. IMRCs possess a unique gene expression profile distinct from umbilical cord mesenchymal stem cells (UCMSCs), such as higher levels of proliferative, immunomodulatory and anti-fibrotic genes. Moreover, intravenous delivery of IMRCs inhibits both pulmonary inflammation and fibrosis in mouse models of lung injury, and significantly improves the survival rate of the recipient mice in a dose-dependent manner, likely through paracrine regulatory

mechanisms. IMRCs are superior to both primary UCMSCs and FDA-approved pirfenidone, with an excellent efficacy and safety profile in mice and monkeys. In light of public health crises involving pneumonia, acute lung injury (ALI) and acute respiratory distress syndrome (ARDS), our findings suggest that IMRCs are ready for clinical trials on lung disorders.

Introduction

Lung injury is a serious threat to human health. It is caused by many chemical, physical and biological agents, resulting in pneumonia, lung inflammation, and fibrosis. In a comprehensive analysis, the World Health Organization ranks lung diseases as the second largest category, and predicts that by 2020, about one fifth of human deaths will be attributed to lung diseases[1]. Acute lung injury (ALI) is the injury of alveolar epithelial cells and capillary endothelial cells caused by various direct and indirect injury factors, resulting in diffuse pulmonary interstitial and alveolar edema, and acute hypoxic respiratory insufficiency. Pathophysiologically, its characteristics include decreased lung volume, decreased lung extensibility and imbalance of the ventilation / blood flow ratio. When ALI develops into the severe stage (oxygenation index < 200), it is called acute respiratory distress syndrome (ARDS). Globally, there are more than 3 million patients with ARDS annually, accounting for 10% of intensive care unit (ICU) admissions[2]. ALI / ARDS patients have an average mortality rate of 35-46%[3,4]. In late ARDS, pulmonary fibrosis (PF) develops due to persistent alveolar injury, repeated destruction, repair, reconstruction and over-deposition of extracellular matrix (ECM)[5], leading to progressive lung scars and common interstitial pneumonia. In general, idiopathic pulmonary fibrosis (IPF) patients show very poor prognosis, with a median survival time of 3-5 years after diagnosis[6]. It has also been reported that the degree of pulmonary fibrosis is closely related to the mortality of ARDS[7,8]. Importantly, there are still no effective FDA-approved drugs to treat ALI, ARDS or IPF hitherto, and most experimental drugs are still in the midst of Phase II or Phase III clinical studies[2, 9,10]. Stem cell therapy is an emerging treatment modality being used to cure various inflammatory and/or degenerative diseases, including ALI and PF. In particular, mesenchymal stem cells (MSCs) have been tested as an intravenous infusion therapy for ALI and PF[11,12]. Preclinical and clinical studies of pulmonary fibrosis have shown that, after infusion, MSCs could migrate to the sites of lung injury, inhibit inflammation and improve recovery[13-15]. However, clinical studies with primary MSCs derived

82 from the umbilical cord, bone marrow or adipose tissue have been hampered by the lack of available
83 donors, limited cell numbers from each donor, donor and tissue heterogeneity, inconsistent cell quality
84 and the lack of standardized cell preparations. Moreover, primary MSCs show limited self-renewal
85 capacities and finite lifespans. MSC-like cells derived from human embryonic stem (hESCs)[16] could
86 solve these problems[17-19], but the use of ill-defined and variable components of animal origin, such as
87 fetal bovine serum (FBS) or OP9 feeder cells, may greatly compromise their consistency, safety and
88 clinical applicability. Furthermore, these hESC-derived MSC-like cells have not been deeply
89 characterized for their immunomodulatory functions in disease models.
90 In this study, we demonstrate that our hESC-derived MSC-like cell population have unique abilities in
91 modulating the immunity and regulating extracellular matrix production, compared to regular MSC
92 populations. Therefore, we named it as immunity- and matrix-regulatory cells (IMRCs). One aspect of
93 IMRCs is that they resemble MSCs in their capacity for self-renewal and tri-lineage differentiation.
94 However, compared to primary umbilical cord mesenchymal stem cells (UCMSCs), IMRCs also
95 displayed a higher consistency in quality, stronger immunomodulatory and anti-fibrotic functions, and
96 a robust ability to treat lung injury and fibrosis in vivo.

97 **Materials and methods**

98 **Generation of hESC-derived IMRCs**

99 The hESC-derived IMRCs were generated by passaging cells that are migrating out from human
100 embryoid bodies (hEBs), with xeno-free reagents. The clinical hESC line (Q-CTS-hESC-2) was
101 prepared as described previously[20]. Clinical hESCs were maintained in commercially available
102 Essential 8™ (E8) basal medium (Gibco, Carlsbad, MO, USA; A15169-01) with Essential 8™
103 Supplement (Gibco, A15171-01) on vitronectin-coated plates (1 μg/cm^2). To generate embryoid bodies
104 (hEBs), hESCs were dissociated into small clumps by incubating at 37°C for 5 min with 1 mg/mL
105 dispase (Gibco, 17105-04) and cultured to form hEBs for 5 days in KO-DMEM (Gibco, A12861-01)
106 supplemented with 20% KOSR (Gibco, A3020902), 1× L-glutamine (Gibco, A12860-01), 1× NEAA
107 (Gibco, 11140050) and 10 ng/mL bFGF (Thermo, 13256029). Then, hEBs were transferred onto
108 vitronectin-coated plates and cultured for 14 additional days. During this period, the outgrowth from
109 the hEBs occurred. The outgrowth cells were dissociated by using Tryple (Gibco, A12859-01) and

110 passaged at a low cell density of 1×10^4 cells per cm^2 in "IMRCs Medium" consisting of α-MEM
111 (Gibco, 12561-049) supplemented with 5% KOSR, 1% Ultroser G (Pall corporation, New York, NY,
112 USA; 15950-017), 1× L-glutamine, 1× NEAA, 5 ng/mL bFGF (Thermo, 13256029) and 5 ng/mL
113 TGF-β3 (Peprotech, 96-100-21-10). Cells were passaged upon reaching approximately 80% confluence
114 in IMRCs Medium. After 5 passages in culture, differentiated cultures were harvested for
115 characterization. By this time, IMRCs displayed a fibroblastic morphology, expressed canonical
116 "MSC-specific" surface markers including CD73, CD90, CD105 and CD29 and were negative for
117 typical hematopoietic markers (CD45, CD34, HLA-DR)[21,22].

118 **Isolation and culture of UCMSCs**

119 Healthy full-term human placental samples were collected according to the policy of the Ethics
120 Committee of the 306th Hospital of the Chinese People's Liberation Army, Beijing, China. Written
121 informed consents were obtained from all donors before this study. All the samples were used in
122 accordance with standard experimental protocols approved by the Animal and Medical Ethical
123 Committee of Institute of Zoology, Chinese Academy of Sciences, Beijing, China.

124 Briefly, the newborn umbilical cords of full-term pregnancies were obtained from the clinic and
125 washed by PBS to remove all remnant blood. Then, the umbilical cords were cut to approximately 2
126 mm in size after removing the artery and vein. The pieces of umbilical cords were directly transferred
127 into a 10 cm^2 culture flasks in α-MEM supplemented with 5% KOSR, 1% Ultroser G, 1× L-glutamine,
128 1× NEAA and 5 ng/mL bFGF, and cultured in an atmosphere of 5% CO_2 at 37°C. UCMSCs were
129 passaged upon reaching approximately 80% confluence. After 5 passages in culture, cells were
130 harvested for characterization.

131 **Cell culture**

132 The clinical hESC line (Q-CTS-hESC-2) was prepared as described previously[20]. Clinical hESCs were
133 maintained in the commercially available Essential 8™ (E8) basal medium on vitronectin-coated plates.
134 Cells were passaged every 5 or 6 days using Versene (Gibco, A4239101). Clinical hESCs were tested
135 weekly for mycoplasma contamination using a Myco-detection Kit (InvivoGen, San Diego, CA, USA;
136 rep-pt1) and endotoxin contamination was tested using a ToxinSensor™ Chromogenic LAL Endotoxin

137 Assay Kit (GenScript, Piscataway, NJ, USA; L00350). All cultures were maintained at 37°C, 5% CO_2
138 and atmospheric O_2 in a humidified incubator (Thermo Fisher Scientific, Waltham, MA, USA). A549
139 cells were purchased from Beina Biology (Shanghai, China). The cells were cultured in Ham's F-12K
140 medium (Gibco, 21127022) with 10% fetal bovine serum (FBS; Gibco, 10091-148) at 37°C in 5% CO_2,
141 and were treated with 10 ng/mL TGF-β1 (R&D systems, 240-B) or IMRCs conditioned medium where
142 specified. To prepare the conditioned medium of IMRCs, IMRCs were cultured to 50% confluence in
143 culture dishes, then, were changed to new medium. The conditioned medium was harvested after
144 incubating IMRCs for 24 h.

145 **Karyotyping**

146 At passage 5, IMRCs were harvested. Karyotype analysis and G-binding were conducted at the
147 Chinese Academy of Medical Science & Peking Union Medical College (Beijing, China).

148 **RNA-seq library preparation and data analysis**

149 Total RNA was isolated from hESCs, IMRCs and UCMSCs by Trizol (Invitrogen, Waltham, MA,
150 USA; 15596018). RNA-seq libraries were prepared with the NEBNext®Ultra™ RNA Library Prep Kit
151 for Illumina®. Sequencing was performed on an Illumina HiSeq X-Ten sequencer with 150 bp
152 paired-end sequencing reaction. The bulk RNA-Seq data for hESCs were downloaded from GEO
153 database[23]. All RNA-sequencing data analysis was performed with Hisat2 (version 2.1.0)[24] and
154 Cufflinks (version 2.2.1)[25] using the UCSC hg19 annotation with default settings. Reads with unique
155 genome locations and genes with no less than 1 FPKM in at least one sample were used for the next
156 step of analysis. Two-fold change was used as the threshold to filter for differentially expressed genes
157 (DEGs) i.e. increased or decreased expression of less than 2-fold was not considered significant. The
158 Gene Ontology analysis for differentially expressed genes was performed by DAVID (version 6.8)[26].
159 Clustering, heatmap, Venn diagram and scatterplots analysis were performed with hierarchical cluster
160 and heatmap.2 functions in R. Pearson correlation coefficient was calculated by cor.test in R. Gene set
161 enrichment analysis were performed by GSEA[27].

162 **Flow cytometry**

Cells were harvested and blocked with 2% bovine serum albumin (BSA; Sigma-Aldrich, B2064) for 20 min at room temperature. Then, the cells were stained with fluorescein-conjugated antibodies for 40 min at room temperature in 1% BSA. After incubation, cells were washed 3 times and analyzed with MoFlo (Beckman, Brea, CA, USA) and associated software. The antibodies used for flow cytometry were as follows: PE-conjugated mouse anti-human CD29 (Biolegend, San Diego, CA, USA; 303004), PE-conjugated mouse anti-human CD73 (BD Biosciences, San Jose, CA, USA; 550257), PE-conjugated mouse anti-human CD90 (eBioscience, San Diego, CA, USA; 12-0909-42), PE-conjugated mouse anti-human CD105 (Biolegend, 323206), PE-conjugated mouse anti-human CD34 (BD Biosciences, 555822), PE-conjugated mouse anti-human CD45 (BD Biosciences, 560957), PE-conjugated mouse anti-human HLA-DR (BD Biosciences, 555561), and the PE-conjugated mouse IgG1 (BD Biosciences, 551436) as an isotype control.

Trilineage differentiation

Osteogenic, adipogenic, and chondrogenic differentiation experiments were performed following the instructions of the human mesenchymal stem cell functional identification kit (R&D systems, SC006). For osteogenic differentiation, 4.2×10^3 cells were seeded per well in 96-well plates. When cells reached 50–70% confluency, the medium was replaced with osteogenic differentiation medium and kept for 3 weeks. To assess osteogenic differentiation, immunofluorescence (Osteocalcin) and Alizarin Red S (Sigma-Aldrich, A5533) staining was performed for the calcium-rich extracellular matrix. For adipogenic differentiation, cells were seeded into a 24-well plate at the density of 3.7×10^4 cells/well, and maintained in culture medium until 100% confluency. Then, cells were cultured in adipogenic differentiation medium for 3 weeks. Lipid droplets of the resultant differentiated cells were detected using immunofluorescence (FABP-4) and Oil red O (Sigma-Aldrich, O0625) staining. For chondrogenic differentiation, 2.5×10^5 cells resuspended in chondrogenic differentiation medium were centrifuged for 5 min at 200×g in a 15-mL conical tube (Corning, NY, USA). Then, cells were cultured for 3 weeks. After 3 weeks, chondrogenic pellet was harvest and fixed in 4% paraformaldehyde (Aladdin Chemical Co., Ltd., Shanghai, China; C104190). Cryosectioning was performed by OTF Cryostat (Leica, Germany) and 10 μm sections were stained with immunofluorescence (Aggrecan) and Alcian Blue (Sigma-Aldrich, A5268) staining.

191 **Growth curve**

192 IMRCs and UCMSCs were seeded onto 96-well plates at a density of 8×10^3 cells per well. Cell
193 Counting Kit-8 (CCK8; Thermo Fisher Scientific, CK04) was used to measure the cells' growth. CCK8
194 solution was added at day 1, day 3, day 5 and day 7 by following the CCK8 kit manufacturer's protocol.
195 After 2 h of incubation, absorbance was measured at 450 nm.

196 **Cell diameter analysis**

197 The IMRCs and UCMSCs were harvested at passage 5 and the cell diameters were measured with
198 Image J software (NIH) software analysis. Normal Distribution curves were fitted to the cell diameter
199 data to analyze the cell size distribution characteristics.

200 **Cell viability test**

201 The IMRCs and UCMSCs were cryopreserved in a published clinical injection[28] for 15 days in liquid
202 nitrogen. After complete recovery of the cells, cells were suspended in clinical injection and remained
203 under 4°C. Then, cell viability was determined using 0.4% (w/v) Trypan Blue (Gbico, 15250061) at
204 different time points by a Cell Counter (Invitrogen, Countess II) using the average of 3 replicates.

205 **Single-cell RNA-seq library preparation & sequencing**

206 IMRCs and UCMSCs were harvested and suspended in PBS. Then, cell suspensions were loaded onto
207 the Chromium Single Cell Controller (10× Genomics) to generate single Gel Beads-in-Emulsion
208 (GEMs) by using Single Cell 30 Library and Gel Bead Kit V2 (10× Genomics, 120237). Cells were
209 lysed and the released RNA was barcoded through reverse transcription in individual GEMs. Following
210 reverse transcription, cDNAs with both barcodes were amplified, and a library was constructed using
211 the Single Cell 30 Reagent Kit (v2 chemistry) for each sample following the manufacture's
212 introduction (performed by CapitalBio Technology, Beijing). Sequencing was performed on an
213 Illumina NovaSeq 6000 System in the 2 × 150 bp paired-end mode. Raw files were processed with Cell
214 Ranger using default mapping arguments. Gene expression analysis and cell type identification were
215 performed by Seurat V3.1. Briefly, after normalizing and quality control, the tSNE was used for

216 non-linear dimensional reduction. The figures were produced by DimPlot and VlnPlot functions in
217 Seurat.

218 **Cell culture with IFN-γ treatment**

219 Cells at passage 4 were digested and seeded into 6-well plates. IMRCs were seeded at a density of 3 ×
220 10^5 cells / well, and UCMSCs were seeded at a density of 2 × 10^5 cells / well. After adherence for 24h,
221 IFN-γ (0, 25, 50, 100 ng/mL) (R&D systems, 285-IF) was added into the culture medium to culture for
222 24h. Cells and conditioned medium were harvested after IFN-γ stimulation for qPCR and cytokine
223 analysis.

224 **Cytokine analysis**

225 Conditioned medium of UCMSCs and IMRCs were collected after IFN-γ (100 ng/mL) stimulation for
226 24h. Forty-eight cytokines including FGF basic, Eotaxin (also known as CCL11), G-CSF (CSF3),
227 GMCSF (CSF2), IFN-γ, IL-1β, IL-1ra, IL2, IL4, IL5, IL6, IL7, IL8 (also known as CXCL8), IL9, IL10,
228 IL12 (p70), IL13, IL15, IL17A, IP10 (CXCL10), MCP1 (CCL2), MIP-1α (CCL3), MIP-1β (CCL4),
229 PDGFB, RANTES (CCL5), TNF-α, VEGF, IL-1α, IL-2Rα, IL-3, IL-12 (p40), IL-16, GRO-α, HGF,
230 IFN-α2, LIF, MCP-3, MIG, β-NGF, SCF, SCGF-β, SDF-1α, CTACK, MIF, TRAIL, IL-18, M-CSF,
231 TNF-β were detected by using the premixed 48-plex Bio-Plex Pro Human Cytokine Assay (Bio-Rad,
232 Hercules, CA, USA; 12007283) according to the manufacturer's instructions.

233 **Lymphocyte proliferation assay**

234 For the proliferation analysis, peripheral blood mononuclear cells (PBMCs) from umbilical cord blood
235 of healthy donors were stimulated by 5 μg/mL phytohaemagglutinin (PHA, Sigma-Aldrich, L4144) in
236 a 96-well plate for 3 days in the presence or absence of IMRCs (2 × 10^5/well) at a ratio of 1:1. At day 3,
237 the proliferation of PBMCs was analyzed by CCK8.

238 **Real-time quantitative PCR**

239 For reverse transcription (RT), RNA was extracted using an RNAprep Pure Cell/Bacteria Kit
240 (TIANGEN, Beijing, China; DP430). Two micrograms of RNA were reverse transcribed into cDNA

241 using a PrimeScript™ First-Strand cDNA Synthesis Kit (TaKaRa, Shiga, Japan; 6110B). Real-time
242 quantitative PCR (qPCR) was performed and analyzed using a Stratagene Mx3005P system (Agilent
243 Technologies, Santa Clara, CA, USA) with SYBR Green Real-Time PCR Master Mix Plus (Toyobo,
244 Osaka, Japan; QPS-201). *GAPDH* was used for internal normalization. Primers for real-time PCR in
245 this study are as shown in Supplementary information, Table S2.

246 **Enzyme-linked immunosorbent assay (ELISA)**

247 To determine the secretion of human MMP1, cell culture supernatants were collected after 48 hours of
248 culture. The levels of human MMP1 protein were measured by a Human MMP1 ELISA Kit (Cusabio,
249 Wuhan, China; CSB-E04672h) according to the manufacturer's instructions. Concentrations of TNF-α
250 (Expandbio, Beijing, China; Exp210030) and TGF-β1 (Expandbio, Exp210089) in the mouse lung
251 homogenates were measured using ELISA kits according to the manufacturer's instructions.

252 **Human MMP1 activity**

253 To determine the activity of human MMP1, cell culture supernatants were collected after 48 hours of
254 culture. The activity of human MMP1 were measured by a SensoLyte® Plus 520 MMP-1 Assay Kit
255 (AnaSpec, San Jose, CA, USA; AS-72012) according to the manufacturer's instructions. A specific
256 anti-MMP-1 monoclonal antibody was used in combination with an MMP1 fluorogenic substrate,
257 5-FAM/QXL®520 FRET peptide. The fluorescence signal is monitored at Ex/Em = 490 nm/520 nm
258 upon MMP-1-induced cleavage of the FRET substrate.

259 **Immunofluorescence staining**

260 Cells were fixed with 4% paraformaldehyde for 15 min, permeabilized with 0.5% Triton X-100 for 15
261 min and blocked with 2% BSA for 60 min at room temperature. Then, the cells were stained with 1:200
262 mouse monoclonal IgG E-cadherin (Abcam, San Francisco, CA, USA; ab1416), 1:200 rabbit
263 monoclonal IgG Collagen I (Cell Signaling Technology, Danvers, MA, USA; 84336), 1:200 rabbit
264 anti-FABP-4 (Thermo Fisher Scientific, PA5-30591), 1:200 rabbit anti-Osteocalcin (Thermo Fisher
265 Scientific, PA5-11849), 1:200 mouse anti Aggrecan (Thermo Fisher Scientific, MA3-16888) overnight
266 at 4°C in 2% BSA in PBS. The cells were washed three times with PBS and then incubated with 1:200
267 Alexa Fluor 488 donkey anti-mouse IgG (H+L) (Jackson ImmunoResearch, West Grove, PA, USA;

268 715-545-151), 1:200 Fluorescein (Cy3) donkey anti-rabbit IgG (H+L) (Jackson ImmunoResearch,
269 711-165-152), 1:200 Fluorescein (Cy3) donkey anti-mouse IgG (H+L) (Jackson ImmunoResearch,
270 715-165-151) or Fluorescein (Cy2) donkey anti-rabbit IgG (H+L) (Jackson ImmunoResearch,
271 711-545-152) secondary antibodies in 2% BSA for 60 min at room temperature in the dark. The
272 washing step was repeated before staining the nuclei with Hoechst 33342 (Invitrogen, H3570).

273 **Western blot**

274 Cells were harvested in RIPA Lysis Buffer (strong) (CWbio, Taizhou, China; CW2333S) containing
275 protease inhibitors (Roche, 4693124001). A total of 40 μg proteins were separated by 4-20% gradient
276 SDS-PAGE gels (GenScript, M42015C) and transferred to PVDF membranes (Millipore, Billerica,
277 MA, USA; IPVH00010). The membranes were blocked at room temperature with 1% BSA for 1 h and
278 incubated overnight at 4°C with primary antibodies: rabbit Collagen I antibody (Cell Signaling
279 Technology, 84336), mouse E-cadherin antibody (Abcam, ab1416), mouse α-SMA antibody
280 (Sigma-Aldrich, A5228) and mouse β-actin antibody (Sigma-Aldrich, A1978). Then, the membranes
281 were washed with TBST for 3 times and incubated for 1 h with a secondary antibody: anti-mouse IgG
282 antibody (HRD) (Sigma-Aldrich, A9044) and anti-rabbit IgG antibody (HRD) (Sigma-Aldrich, A0545)
283 at room temperature. Images were obtained using the ChemiDoc XRS+ imaging system (Bio-Rad) and
284 quantified using the Quantity One software.

285 **Soft agar colony formation assay**

286 Soft agarose gels were prepared according to previously published protocols[29]. Cells were harvested
287 and diluted to a cell concentration of 2.5×10^4/mL, before mixing with the agarose mixture in 6-well
288 culture plates. The plates were incubated in a 37°C incubator for 21 days.

289 **Animals**

290 Adult female and male cynomolgus monkeys (3–5 years old) were housed in single quarters with a
291 12/12-hr light/dark cycle. Animals were provided with monkey chow and enrichment food twice a day
292 and water *ad libitum*. The monkey experiments were performed at the National Center for Safety
293 Evaluation of Drugs, National Institutes of Food and Drug Control (Beijing, China). The Institutional

Animal Care and Use Committee of the National Center for Safety Evaluation of Drugs approved all monkey studies (NO. IACUC- 2018- k001).

Specific pathogen-free (SPF) 11- to 13-week-old C57BL/6 male mice were purchased from the Animal Center of Peking University (Beijing, China). All experimental and control mice were weight-matched, and their weights ranged from 25 to 30 g. All mice were housed in the animal care facility of the Institute of Medical Science, China-Japan Friendship Hospital. Mice were maintained under SPF conditions at room temperature (between 20–24°C), with humidity between 35–55%, in a 12/12 h light/dark cycle, with food and water *ad libitum* and monitored with respect to their general state, fur condition, activity, and weight according to institutional guidelines. The mice were sacrificed at each observational time point by using intraperitoneal pentobarbital overdose. The Animal Studies Committee of the China-Japan Friendship Hospital (Beijing, China) approved all mice studies (NO.190108).

Acute toxicity and long-term toxicity test

Acute toxicity test: Low dose (2.6×10^6), middle dose (2.6×10^7) and high dose (1×10^8) IMRCs were infused into cynomolgus monkeys (3-5 years old) by single intravenous infusion. After 6 months, their body weight, ophthalmology status, hematology, blood chemistry and urine chemistry were measured.

Long-term toxicity test: High dose (1×10^7) and low dose (2.6×10^6) IMRCs, or saline, were injected into cynomolgus monkeys (3-5 years old) by intravenous infusion once a week for 22 times, after which their body weight, body temperature, food intake and organ weights were measured.

Copy number variation calling

30X whole-genome sequencing data was produced by HiSeq X-Ten (Annoroad Gene Technology Co., Ltd) and used to analyze single nucleotide mutation changes between IMRCs and hESCs. As previously described[30], the whole-genome sequencing data was mapped to the hg19 reference genome by BWA (version 0.7.15) using the 'mem' mode with default parameters. The genome coverage was calculated by bedtools[31]. The normalized coverage depth for each bin was calculated by dividing the raw coverage depth by the average sequencing depth. Duplicate reads were removed and the uniquely mapped reads were retained for the copy-number variation (CNV) analysis, in which chromosomal

321 sequences were placed into bins of 500 kb in length. The hg19 genome repeat regions annotated by
322 RepeatMasker (http://www.repeatmasker.org) were removed from the genomic sequence before
323 calculating the coverage. The CNV scatterplot was drawn using ggplot2.

324 **Histological staining and immunostaining staining analysis**

325 Mouse lung histology was performed as follows. Briefly, the lung was dehydrated, paraffin-embedded
326 and cut into 4 μm sections. Lung sections were stained with H&E and Masson's trichrome stain for
327 assessment of pathological changes. Immunohistochemical staining was performed using antibodies
328 against α-SMA (Servicebio, Wuhan, China; GB13044), Fibronectin (Servicebio, GB13091), Collagen I
329 (Servicebio, GB13091) and GFP (Servicebio, GB13227). Immunofluorescence staining was performed
330 using antibodies against GFP (Servicebio, GB13227), CD31 (Servicebio, GB11063-3) and SPC
331 (Millipore, AB3786).

332 **Labeling IMRCs with DiR dye**

333 IMRCs were labeled with a lipophilic, near-infrared fluorescent dye 1,1-dioctadecyl-
334 3,3,3,3-tetramethyl indotricarbocyanine iodide (DiR; YEASEN, Shanghai, China; 40757ES25). IMRCs
335 were suspended at a concentration of 1×10^6 cells / mL and incubated with DiR buffer for 20 min at
336 37°C according to the manufacturer's protocol. After incubation, cells were centrifuged at 1000-1500
337 rpm for 5 min. After washing twice with PBS and resuspension, the IMRCs were preheated at 37°C
338 before infusion. Both DiR-labeled and unlabeled cells (5×10^6 in 200 μL saline) were injected via the
339 tail vein.

340 **In vivo imaging of IMRCs' biodistribution**

341 Mice were lightly anesthetized and were monitored using the in vivo imaging systems at 0 day, 1 day, 3
342 days, 5 days, 7 days, 9 days, 15 days, 21 days, 27 days, 32 days, 37 days and 46 days after tail
343 intravenous injection of DiR-labeled IMRCs (5×10^6 cells in 200 μL saline). Serial fluorescence images
344 were also obtained in major organs ex vivo. In order to reduce autofluorescence, the ideal filter
345 conditions for DiR imaging were an excitation/emission spectrum in the near infrared range (750/780
346 nm)[32,33].

347 **Lung function**

348 The flexiVentFX experimental platform was set up according to the manufacturer's instructions. On the
349 twenty-first day, after 3% pentobarbital sodium (40 mg/kg) intraperitoneal injection of anesthesia, mice
350 were fixed supine within five to eight minutes, and endotracheal intubation was inserted in the middle
351 of a tracheotomy. After computer processing, indicators of lung function required were obtained,
352 including the inspiratory capacity (IC), respiratory resistance (Rrs), static compliance (Crs), elastic
353 resistance (Ers), Newtonian resistance, tissue damping (G), tissue elasticity (H) and forced vital
354 capacity (FVC)[34].

355 **Lung coefficient**

356 The lung tissue was completely removed, weighed by electronic balance, and the lung coefficient was
357 calculated according to the formula: wet lung weight (g) / total body weight (kg).

358 **Cell therapy in BLM mouse model of pulmonary fibrosis**

359 The BLM mouse model was generated by intratracheal injection of 1.5 $mg.kg^{-1}$ bleomycin sulphate
360 (BLM; Bioway, China; DP721) in normal saline under light anaesthesia. The IMRCs were delivered
361 intravenously at 0 day or 1 day or 7 days or 14 days after injury. Mice were euthanized with 50 mg/mL
362 sodium pentobarbital (0.6 mg/10 g weight) according to published guidelines[35]. Animals were killed 21
363 days after BLM injury. After perfusion with normal saline, the left lungs were used for morphometric
364 analysis while the right lungs were removed and used for other analyses.

365 **Micro-CT**

366 Mouse CT scans were performed according to the manufacturer's instructions.

367 **Compassionate use study of two severely ill COVID-19 patients**

368 We conducted a pilot study using GMP-grade IMRCs, under an expanded access program for
369 compassionate use in COVID-19 patients. The pilot study was approved by the Ethics Committee of
370 the Beijing Youan Hospital, Capital Medical University (LL-2020-010-K, Youan EC [2020]005). After

371 two severely ill COVID-19 patients, who tested positive for SARS-CoV-2 by qRT-PCR and were
372 diagnosed with ALI (aged 44–46 yrs; 1 male and 1 female), gave their consent and met the eligibility
373 criteria, their serum samples were collected and processed in accordance with the ethical legislation
374 and the guidelines of the Ethics Committee of the Beijing Youan Hospital, Capital Medical University.

375 **Statistics**

376 All data are expressed as mean ± SEM. Survival curves were derived by the Kaplan-Meier method and
377 compared via generalised Wilcoxon test. Statistical analysis was performed using GraphPad Prism 5.0
378 statistical software (San Diego, CA, USA). The statistical significance of multiple groups was
379 compared to each other using Tukey's multiple comparison test ANOVA. A p value of < 0.05 was
380 considered statistically significant.

381

382 **Results**

383 **Generation of hESC-derived IMRCs**

384 In this study, hESC-derived IMRCs were generated by passaging cells that are migrating from human
385 embryoid bodies (hEBs), using xeno-free reagents (Fig. 1a, b). The clinical hESC line (Q-CTS-hESC-2)
386 was prepared as described previously[20]. Clinical hESCs were maintained in Essential 8™ basal
387 medium (E8) on vitronectin-coated plates, before dissociation into small clumps to form hEBs for 5
388 days. Subsequently, hEBs were transferred onto vitronectin-coated plates and cultured for 14 additional
389 days. The hEBs outgrowth cells were dissociated and passaged continuously in IMRCs Medium. After
390 5 passages, IMRCs were harvested for characterization. IMRCs possessed fibroblast-like morphology
391 (Fig. 1b) and maintained diploid karyotypes at passage 5 (Fig. 1c). Moreover, copy-number variation
392 analysis by whole genome sequencing data also indicated that no chromosomal aneuploidies, large
393 deletions nor duplication fragments were detected (Fig. 1d). Next, we analyzed the expression profile
394 of MSC-specific genes (Fig. 1e). IMRCs showed a pattern that greatly differed from hESCs, and
395 closely resembled primary umbilical cord-derived MSCs (UCMSCs). All pluripotency genes (*POU5F1*,
396 *SOX2, NANOG, ZFP42, SALL4*), mesendoderm genes (*MIXL1*), and ectoderm genes (*GAD1*) were
397 extinguished in both IMRCs and UCMSCs (Fig. 1e). IMRCs expressed MSC-specific genes, including

398 *PDGFRA* and *SPARC,* and the MSC-specific surface markers *NT5E* (CD73), *ENG* (CD90), *THY1*
399 (CD105) and *ITGB1* (CD29). Flow cytometry analysis further confirmed this surface marker profile
400 (Fig. 1f; Supplementary information, Fig. S1a, b). By contrast, IMRCs were negative for the
401 hematopoietic surface markers *PTPRC* (CD45) and CD34. IMRCs displayed the ability to undergo
402 tri-lineage differentiation into mesenchymal tissues, such as adipose, cartilage and bone cells (Fig. 1g;
403 Supplementary information, Fig. S1c). The proliferation rate of IMRCs was higher than that of
404 UCMSCs at passage 15, suggesting that IMRCs have a stronger capacity for long-term self-renewal
405 than primary MSCs (Fig. 1h). Interestingly, IMRCs were generally smaller than UCMSCs (Fig. 1i),
406 suggesting that IMRCs can pass through small blood vessels and capillaries more easily, and are thus
407 perhaps less likely to cause pulmonary embolism. To evaluate the clinical potential of the IMRCs, we
408 measured the viability of IMRCs suspended in a published clinical injection buffer at 4°C. We found
409 that the viability of IMRCs remained higher (93%) than UCMSCs (73%) after 48h (Fig. 1j).

410 **IMRCs possess unique gene expression characteristics**

411 To clarify the degree of similarity between hESCs, IMRCs and primary UCMSCs at the whole
412 transcriptome level, we performed genome-wide profiling of IMRCs and UCMSCs and compared their
413 gene expression with hESCs[23]. Whole-transcriptome analysis confirmed that IMRCs clustered together
414 with UCMSCs in an unsupervised hierarchical clustering (Fig. 2a). The global differential expressed
415 gene analysis showed that highly expressed genes in IMRCs and UCMSCs compared with hESCs,
416 were enriched with angiogenesis, inflammatory response and extracellular matrix disassembly related
417 processes (Supplementary information, Fig. S2). Accordingly, MSC-specific genes such as *NT5E, ENG,*
418 *PDGFRA, SPARC* and *ITGB1* were upregulated, whereas pluripotency genes such as *POU5F1, SOX2,*
419 *SALL4* and *ZFP42* were extinguished in IMRCs relative to hESCs, and the overall correlation with
420 hESCs was weak (R^2=0.66; Fig. 2b). Next, we analyzed for the expression of genes specific to IMRCs,
421 compared to UCMSCs (Fig. 2c). While the overall correlation with UCMSCs was stronger (R^2=0.87),
422 we also found that many genes were differentially expressed in IMRCs compared to primary UCMSCs.
423 The upregulated genes promote immunomodulation (*LIF*), tissue repair (*VEGFA, GREM1*), cell
424 division (*CDC20*) and anti-fibrosis (*MMP1*). By contrast, the downregulated genes predominantly
425 promote inflammation (*IL-1B, CXCL8, CCL2* and *CXCL1;* Fig. 2c). Gene set enrichment analysis

426 (GSEA) of the differentially expressed genes confirmed that IMRCs manifest reduced inflammation
427 and stronger proliferative capacity as their top gene signatures, compared to primary UCMSCs (Fig. 2d,
428 e; Supplementary information, Fig. S3).
429 To elucidate the heterogeneity of gene expression amongst IMRCs, single cell RNA sequencing
430 (scRNAseq) was performed for both IMRCs and primary UCMSCs. A total of 16000 single-cell
431 transcriptomes were obtained from two samples. Approximately ~100000 reads were obtained per cell,
432 which generated a median of 31000 unique molecular identifiers per cell, ~4800 expressed genes per
433 cell and more than 22000 total genes detected in the population. Our scRNAseq data also showed that
434 IMRCs were relatively homogenous in expression for the MSC-specific markers *PDGFRA, SPARC,*
435 *NT5E, ITGB1* and *ENG* (Fig. 2f; Supplementary information, Fig. S4). IMRCs were also relatively
436 homogenous in their suppression of pluripotency and non-mesenchymal markers, relative to hESCs
437 and UCMSCs, suggesting they are likely to be similar in biological activity to primary MSCs after
438 transplantation (Fig. 2g; Supplementary information, Fig. S4). These results provided insight into the
439 clinical applicability of IMRCs, especially with regards to their complete loss of pluripotency and their
440 gain in hyper-immunomodulatory potential.

441 **IMRCs treated with IFN-γ show hyper-immunomodulatory potency**

442 To test the immunomodulatory capacity of IMRCs, we exposed them to the pro-inflammatory cytokine
443 IFN-γ. We found that after stimulation with IFN-γ, both primary UCMSCs and IMRCs displayed
444 similar characteristic morphological changes (Fig. 3a). IFN-γ stimulation also potently upregulated
445 *IDO1* (indoleamine 2, 3-dioxygenase 1) expression in both primary UCMSCs and IMRCs, but much
446 more significantly so in IMRCs (Fig. 3b). This is important because *IDO1* has been shown to mediate
447 immunosuppression in T cell-inflamed microenvironments through its catabolism of tryptophan and
448 thus suppression of the tryptophan–kynurenine–aryl hydrocarbon receptor (Trp–Kyn–AhR) pathway in
449 T cells. To further characterize IMRCs at a molecular level, we conducted genome-wide RNA profiling
450 to compare IMRCs with UCMSCs, after IFN-γ stimulation (Fig. 3c). Hierarchical clustering revealed
451 that IMRCs clustered separately from UCMSCs, although they appeared more similar after IFN-γ
452 stimulation (Fig. 3d). To analyse IMRCs after IFN-γ stimulation in greater detail, we separated their
453 differentially expressed genes into different categories and tested their overlap using Venn diagram

454 analysis (Fig. 3e). The global differential expressed gene analysis showed that highly expressed genes
455 in IMRCs and UCMSCs after IFN-γ stimulation, compared with IMRCs and UCMSCs before IFN-γ
456 stimulation, were enriched with immune response and interferon-gamma-mediated signaling pathway
457 (Supplementary information, Fig. S5). Accordingly, we found that some pro-inflammatory genes
458 showed lower expression while some pro-regenerative genes showed higher expression levels in
459 IMRCs, compared to primary UCMSCs (Fig. 3f).
460 To confirm these findings, we performed a focused ELISA analysis of 48 biologically relevant
461 chemokines and cytokines in the secretomes of both stimulated IMRCs and UCMSCs. We found that at
462 least nine pro-inflammatory cytokines were lower in IMRCs than UCMSCs, including interleukin-6
463 (IL-6), IL-1b, tumor necrosis factor alpha (TNF-α), GRO-α, IFN-α2, IL-1α, IL-3, and IL-8 (Fig. 3g;
464 Supplementary information, Fig. S6a). Furthermore, while the anti-inflammatory IL-4 was lower, the
465 immunomodulatory cytokines IL-1RA, LIF, and RANTES were higher in IMRCs than UCMSCs (Fig.
466 3h). Amongst the pro-regenerative cytokines, we found that GM-CSF was similar while VEGFA, MIG
467 and SDF-1a were higher in IMRCs than UCMSCs (Fig. 3i). To determine the immunomodulatory
468 properties of IMRCs, we examined the effects of IMRCs on PBMCs' proliferation and found that
469 IMRCs significantly inhibited PHA-stimulated PBMCs' proliferation when cocultured together at a
470 ratio of 1:1 (Supplementary information, Fig. S6b). These results indicate that IMRCs manifest much
471 stronger immunomodulatory and pro-regenerative functions than UCMSCs.

472 **IMRCs suppress the pro-fibrotic effects of TGF-β1**

473 Our scRNAseq results also indicated that more than 99% of IMRCs expressed *MMP1* compared with
474 primary UCMSCs (<1%) (Fig. 4a; Supplementary information, Fig. S4). Similarly, gene expression
475 analysis by RT-qPCR showed that IMRCs express much higher levels of *MMP1* than hESCs, UCMSCs
476 or human foreskin fibroblasts (HFF; Fig. 4b). MMP1 could be detected as a highly secreted protein in
477 the conditioned media of IMRCs by ELISA (Fig. 4c). In addition, the secreted MMP1 was an
478 enzymatically active and correctly processed isoform (Fig. 4d, e). To investigate the role of the IMRCs
479 on fibrosis, the human epithelial cell line A549 was used to establish an in vitro fibrosis model. The
480 morphology of A549 cells became myofibroblast-like after 48h treatment with 10 ng/mL TGF-β1 (Fig.
481 4f). Consistent with the morphological changes, the expression of myofibroblast markers such as

482 *ACTA2*, *Collagen I*, *Collagen II*, *Fibronectin* and *TGFB1* increased, while the expression of the
483 epithelial identity marker *CDH1* was extinguished, suggesting that the A549 cells had undergone
484 TGF-β1-induced myofibroblast transdifferentiation (Fig. 4g). Immunofluorescence and western blot
485 analyses confirmed that TGF-β1 induced the upregulation of collagen I and the downregulation of
486 E-cadherin (Fig. 4h, i). These results indicated that the A549 alveolar epithelial cells could simulate
487 lung fibrosis in vitro. Thereafter, A549 cells were cultured with or without the conditioned media of
488 IMRCs, along with TGF-β1 treatment. Our results showed that the IMRC conditioned media
489 significantly ameliorated the induction of *Collagen I*, *ACTA2* and *TGFB1* expression (Fig. 4j;
490 Supplementary information, Fig. S7a). Immunofluorescence and western blot analyses further
491 confirmed that IMRC conditioned media could extinguish Collagen I protein expression and inhibit
492 α-SMA protein expression during the A549-to-myofibroblast transdifferentiation (Fig. 4k-m;
493 Supplementary information, Fig. S7b, c). These results suggested that IMRCs might be able to inhibit
494 lung fibrosis.

495 **Safety evaluation of IMRC transfusion into mice and monkeys**

496 Tumorigenicity has long been an obstacle to the clinical application of cells derived from hESCs, due
497 to the contamination of residual hESCs that could form teratomas. Our single cell RNA sequencing
498 showed that no residual OCT4/SOX2/NANOG/TERT/DPPA5^{+} hESCs remained amongst the IMRCs,
499 and that all pluripotency gene expression had been extinguished (Fig. 5a). To ensure their short-term
500 and long-term safety, a series of biosafety-related experiments were performed according to the
501 "Guidelines for Human Somatic Cell Therapies and Quality Control of Cell-based Products" of China
502 Food and Drug Administration (CFDA) (http://samr.cfda.gov.cn/WS01/CL0237/15709.html),
503 whereupon the IMRCs were verified as suitable for use in human therapy (Supplementary information,
504 Table S1). These biosafety-related experiments included testing for bacteria, fungi, mycoplasma, virus
505 (by in vivo and in vitro methods), pluripotent cell residuals, tumorigenicity and biopreparation safety
506 (endotoxin and bovine serum albumin residuals). According to these tests, the safety of the IMRCs has
507 been verified as required by the National Institutes for Food and Drug Control (NIFDC) in China.
508 To track the biodistribution and long-term engraftment of IMRCs in vivo, whole-animal imaging of
509 wildtype mice was performed at designated time points (day 0, 1, 3, 5, 7, 9, 15, 21, 27, 32, 37 and 46)

510 after injection with DiR-labeled IMRCs (Supplementary information, Fig. S8a). Our data showed that
511 DiR fluorescence intensity declined by half on the 5th day, and dropped steadily over at least 15 days,
512 disappearing around day 46 (Fig. 5b, c; Supplementary information, Fig. S8c). No DiR fluorescence
513 signals were observed in the control mouse. These results indicate that IMRCs never show long-term
514 engraftment in vivo. However, IMRCs were predominantly distributed to the lung, with small amounts
515 in the liver and spleen (Supplementary information, Fig. S8b). To assess the recruitment of IMRCs to
516 the lung in greater detail, GFP-labeled IMRCs were used to track the distribution of IMRCs. A number
517 of GFP-labeled IMRCs were observed in the interstitial spaces in the lung, but not in the lung
518 capillaries (Fig. 5d). Immunofluorescence analysis of the expression of the alveolar type II epithelial
519 cell marker SPC and the endothelial cell marker CD31 showed that neither marker was co-expressed
520 with GFP-labeled IMRCs in the lungs of mice by day 21 (Fig. 5d). These data suggested that IMRCs
521 are unlikely to engraft nor transdifferentiate into endothelial or epithelial cells, after homing to the
522 interstitium of lung tissues in vivo.
523 To give some indication of the tumorigenic potential of IMRCs in vitro, a soft agar assay was
524 performed (Fig. 5e). As a positive control, the PANC-1 pancreas tumor cell line showed a colony
525 formation rate of about 30%. A small number of clones were also formed by hESCs, and the colony
526 formation rate was about 0.5%. However, no colonies were formed by IMRCs. These results indicated
527 that IMRCs had no tumorigenic potential as determined by this assay. Somatic mutation analysis by
528 whole genome sequencing also showed zero mutations in all coding and noncoding exon regions of the
529 IMRCs genome (Fig. 5f). Tumor formation assays also confirmed that IMRCs could not form any
530 tumors in immunodeficient mice after injection in vivo (Supplementary information, Table S1).
531 We also transfused different doses of IMRCs into cynomolgus monkeys (*Macaca fascicularis*), to
532 evaluate the short- and long-term toxicity of IMRCs in primates. After 6 months, acute toxicity data
533 showed that all blood biochemistry and urinalysis markers remained in the normal range (Fig. 5g, h;
534 Supplementary information, Fig. S9a), indicating normal liver, kidney, heart, muscular, pancreatic and
535 overall metabolic functions. Moreover, no abnormalities were observed in the long-term toxicity tests
536 either, suggesting minimal xenogeneic rejection responses (Supplementary information, Fig. S9b;
537 n=18). These results indicated that IMRCs have a robust safety profile in vitro and in vivo, and could
538 potentially provide therapeutic treatments with good safety levels for clinical potential.

539 **IMRC transfusion treats lung injury and fibrosis in a dose-dependent manner**

540 To evaluate the therapeutic effects of IMRCs on lung injury and fibrosis, IMRCs were administered
541 intravenously into a bleomycin-induced model of lung injury (Fig. 6a). IMRCs ameliorated the total
542 body weight reduction in mice exposed to bleomycin (BLM)-induced lung injury, in a dose-dependent
543 manner (Fig. 6b). Kaplan-Meier survival curves indicated that IMRC treatment prolonged the overall
544 survival rates (BLM group 12.5% vs. 1×10^6 IMRCs 25%, 3×10^6 IMRCs 50%, 5×10^6 IMRCs 62.5% (P
545 < 0.01)) and the median survival time (BLM group 11.5d vs. 1×10^6 IMRCs 15.5d, 3×10^6 IMRCs 18d,
546 5×10^6 IMRCs 21d) in mice exposed to bleomycin-induced lung injury. There was a statistically
547 significant difference between the BLM group and the 5×10^6 IMRCs group, but not the other groups
548 (Fig. 6c). Histological staining of the lung at 21 days after bleomycin injection (inflammation phase)
549 showed diffuse pneumonic lesions with loss of the normal alveolar architecture, septal thickening,
550 enlarged alveoli, and increased infiltration of inflammatory cells in the interstitial and peribronchiolar
551 areas, in the BLM lung compared with normal lung. IMRC treatment reduced alveolar thickening in
552 the lung in a dose-dependent manner (Fig. 6d-f). Moreover, IMRC treatment reduced the number of
553 macrophage in the lung (Fig. 6f). These results indicated that IMRC treatment can reduce inflammation
554 in the lung after acute injury. Moreover, IMRC treatment also improved the Ashcroft score for
555 pulmonary fibrosis in a dose-dependent manner (Fig. 6g). In particularly, IMRC treatment decreased
556 collagen deposition in the BLM lung in a dose-dependent manner (Supplementary information, Fig.
557 S10b, f). The expression levels of COL I, FN and α-SMA were also significant lower after IMRC
558 treatment (Supplementary information, Fig. S10). ELISA showed that IMRC treatment reduced both
559 TNF-α and TGF-β1 levels in the BLM lung in a dose-dependent manner (Fig. 6h, i). These results
560 suggested that IMRCs can significantly reduce inflammation and fibrosis after lung injury, in a
561 dose-dependent manner.

562 **IMRC treatment of lung injury and fibrosis is superior to UCMSCs and pirfenidone injections**

563 Pirfenidone (PFD) is an FDA-approved drug for the treatment of idiopathic pulmonary fibrosis. It
564 works by reducing lung fibrosis through downregulating the production of growth factors and
565 procollagens I and II. To evaluate the efficacy of IMRC treatment, we compared it side-by-side with
566 UCMSCs and PFD treatments of BLM-injured mice (Fig. 6j). Our results showed that IMRC treatment

567 led to an improved amelioration of the weight reduction after BLM-induced lung injury, compared to
568 UCMSCs or PFD treatments (Fig. 6k). Kaplan-Meier survival curves indicated that the IMRC
569 treatments also resulted in the highest overall survival rates compared to UCMSCs or PFD treatments
570 (BLM group 39.02%, vs. IMRCs 70% ($P<0.01$), UCMSCs 52.63%, PFD 65% ($P < 0.05$); Fig. 6l).
571 Moreover, IMRC treatment showed the best improvement in lung morphology (Supplementary
572 information, Fig. S11a) and the best reduction in BLM-induced edema, as measured by the lung
573 coefficient (lung wet weight/total body weight), compared to UCMSCs or PFD treatments
574 (Supplementary information, Fig. S11b).
575 Functionally, mice treated with IMRCs showed the best improvements in indices for lung capacity,
576 including pressure-volume (PV), inspiratory capacity (IC), static compliance (Crs) and forced vital
577 capacity (FVC) (Supplementary information, Fig. S12a-d). IMRC treatment also showed the best
578 reduction in functional indices for lung fibrosis, including respiratory resistance (Rrs), elastic resistance
579 (Ers), tissue damping (G) and tissue elasticity (H) were observed (Supplementary information, Fig.
580 S12e-h). Computed tomography (CT) scans also showed that IMRC treatment led to the best
581 improvement in lung morphology, compared to UCMSCs or PFD treatment (Supplementary
582 information, Fig. S12i, j). In fact, measurements of the lung volume indicated that mice treated with
583 IMRCs had the best improvement in lung volume compared to UCMSCs or PFD treatments. These
584 results indicated that the IMRC therapy is superior to primary UCMSCs and pirfenidone in treating
585 lung injury and fibrosis.
586 Encouraged by these results, and in response to the urgency of the COVID-19 crisis in China, we
587 pilot-tested IMRC transfusion as compassionate treatments in two severely ill COVID-19 patients who
588 were diagnosed with ALI, as part of an expanded access program. After patient consent, IMRCs were
589 administered intravenously in both severely ill patients. Within 14 days after IMRC transfusion, both
590 the severely ill COVID-19 patients showed significant recovery from pneumonia, tested negative for
591 SARS-CoV-2, and were recommended for discharge. Cytokine analysis of both patients' plasma
592 showed very high levels of inflammatory cytokines initially in days 1-2, as expected of the
593 ALI-induced cytokine release syndrome that was manifesting at the point of treatment (Fig. 6m).
594 However, by days 4-8, many pro-inflammatory cytokines were suppressed after IMRC infusion,
595 including GRO-α, IFN-α2, IL-3, IL-9, IL-13, MCP-3, M-CSF, sCD40L and TNF-α (Fig. 6m). These
596 results suggested that IMRCs might possess a hyper-immunomodulatory function with potential

597 therapeutic benefits to ALI patients without other treatment options.

598 **Discussion**

599 In this study, IMRCs were derived from self-renewing hESC cultures with xeno-free reagents. Our
600 results showed that IMRCs, while similar to primary UCMSCs, were superior in their long-term
601 proliferative capacity, hyper-immunomodulatory and anti-fibrotic functions. In addition, the cell
602 diameters of IMRCs were generally smaller than UCMSCs, suggesting that they pose lower risks for
603 pulmonary embolism after injection. Detailed analysis of mice and monkeys after IMRC injections
604 indicates that IMRCs do not engraft, nor transdifferentiate nor initiate tumorigenesis, showing excellent
605 potential for short- and long-term safety profiles by a range of in vitro and in vivo assays. Most
606 importantly, our experiments with the bleomycin mouse model of lung injury showed that treatments
607 with IMRCs are superior to primary UCMSCs and the FDA-approved pirfenidone in therapeutic
608 efficacy.
609 In recent years, MSC-like cells have been generated from hESCs using various protocols[18,19,36,37].
610 However, to the best of our knowledge and in spite of significant efforts by numerous groups,
611 previously reported studies lacked biosafety-related experiments. This has hindered their translation to
612 clinical application. To ensure safety, a series of biosafety-related experiments were performed
613 according to the "Guidelines for Human Somatic Cell Therapies and Quality Control of Cell-based
614 Products" and the IMRCs were verified as suitable for use in human therapy. Our data showed that
615 there was no teratoma formation observed after IMRC injection into the testes of NOD-SCID mice. In
616 addition, single cell RNA sequencing data showed no residual hESCs were detected in IMRCs and soft
617 agar assays also showed that no colonies were formed by IMRCs. In addition, the somatic mutation
618 analysis by whole genome sequencing also showed no mutations in proto-oncogenes and tumor
619 suppressor genes, nor any coding and non-coding exon regions of IMRCs. These results indicated that
620 IMRCs have no demonstrable potential to form tumors. Moreover, IMRCs could not undergo
621 long-term engraftment and disappeared around day 46. IMRCs did not transdifferentiate into
622 endothelial cells nor alveolar epithelial cells in the lung. To evaluate the risks of clinical application,
623 short- and long-term toxicity tests were performed in cynomolgus monkeys. After 6 months, both acute
624 toxicity tests and long-term toxicity test data showed that no abnormalities were observed. These

results proved that IMRCs could have an excellent safety profile and clinical potential. Moreover, the above data suggested that the therapeutic efficacy of IMRCs may not be due to long-term engraftment and direct repair of tissue, but due to their hyper-immunomodulatory and anti-fibrotic functions at inflammatory sites of tissue interstitium.

Like MSCs, the IMRCs are immunoprivileged, and can escape allogeneic immune responses through their lack of expression of HLA class II and their weak expression of HLA class I, thus making them valuable choices for allogeneic cell therapy. Moreover, it has been reported that MSCs could release immunomodulatory factors, alter the expression of surface molecules, and produce growth factors during an immune response to the inflammatory cytokines produced by T cells and antigen-presenting cells[38]. These immunomodulatory factors are crucial for regulating the immune system and promoting tissue repair. Accordingly, expression of the T cell-suppressive *IDO1* greatly increased in IMRCs after stimulation with the pro-inflammatory cytokine IFN-γ, even more than primary MSCs. Genome-wide RNA sequencing revealed that IMRCs and UCMSCs had different expression profiles after exposure to IFN-γ. Analysis of the secretomes of IMRCs and UCMSCs confirmed at least nine pro-inflammatory cytokines that were lower, and several anti-inflammatory cytokines and pro-regenerative factors that were higher in IMRCs than UCMSCs. All these results suggested that IMRCs possess a hyper-immunomodulatory capacity compared to primary UCMSCs, after stimulation with IFN-γ. Thus, these cells can be administered to immunocompetent animals and human patients without the need for further immunosuppression.

Moreover, higher levels of MMP1 were secreted by IMRCs than primary UCMSCs. MMP1 plays a very important role in the process of fibrosis, by degrading existing collagens and promoting the early stages of tissue remodeling that are critical for the progression of fibrogenesis[39,40]. In general, an imbalance between MMPs and TIMPs is the direct cause of fibrosis and tissue scarring. It has been reported that transplantation of human *MMP1*-overexpressing bone marrow-derived mesenchymal stem cells can attenuate CCL4-induced liver fibrosis in rats[41]. Therefore, it is conceivable that IMRCs that highly express MMP1 may also reverse lung fibrosis. Accordingly, our data showed that the secretome from IMRCs could reduce collagen I levels during fibrogenesis induced by TGF-β1. However, it is still unclear whether MMP1 played a direct role in the decrease of collagen I. Future work will focus on the role of MMP1 by using *MMP1*-knockout IMRCs in vitro and in vivo.

The mouse BLM model is similar to human ALI/ARDS during the acute inflammatory phase. Although

655 fibroblastic foci, alveolar epithelial type 2 cells hyperplasia and honeycombing lesions are reduced
656 compared with those in humans, indicating that the modeling of human ARDS is not complete in the
657 mouse BLM model, injury to alveolar epithelial cells has been shown to be a common contributing
658 factor to the pathogenesis of both human ARDS and BLM-induced mouse pulmonary injury[41,42]. To
659 test the therapeutic efficacy of IMRCs in the BLM mouse model, the delivery route and schedule of
660 administration (e.g. single dose versus repeated doses) were carefully considered. Intravenous infusion
661 is one of the principal delivery routes, considered to be minimally invasive, simple to use, and is the
662 most common mode for primary MSCs delivery in diverse lung disorders[43,44]. Furthermore, systemic
663 intravenous transplantation may be a suitable administration route in other future clinical scenarios. In
664 our present study, intravenous IMRCs improved the survival rate of mice with BLM-induced lung
665 injury in a dose-dependent manner, by inhibiting both pulmonary inflammation and fibrosis. As
666 demonstrated in vitro, IMRCs inhibited the production of pro-inflammatory cytokines and pro-fibrosis
667 cytokines, such as TNF-α and TGF-β1, in lung tissue in vivo. Furthermore, lung function indicators
668 such as PV, IC, Rrs, Crs, Ers, Rn, G, H and FVC were improved compared with the BLM group.
669 It should be noted that IMRCs were administered at 1 and 7 days after initiation of BLM-injury, but
670 before fibrosis has fully developed. In fact several studies have reported that primary MSCs treatments
671 do not improve pre-established pulmonary fibrosis, while some studies suggest that primary MSCs
672 actually exacerbate pulmonary fibrosis[45]. Regarding the efficacy of IMRCs in established fibrosis,
673 further studies are necessary and our own investigation is still ongoing. It is unclear whether primary
674 MSCs do promote pulmonary fibrosis, but their lack of positive therapeutic effect may be due to
675 differences in MSC subtypes and functions, fibrosis stages after induction, species of model animals,
676 and routes of administration of MSCs. Thus, clinical applications with MSCs should be considered
677 carefully. As noted in this study, it is important to carefully document the origin, preparation and
678 characterization of MSC-like cells. Here we have established a substantial profile of efficacy and safety
679 for the hESC-derived IMRCs. These efforts provide considerable grounds for hope that this artificial
680 cell-type could provide significant clinical benefit in the treatment of inflammatory and fibrotic disease
681 conditions.

682 **Conclusions**

In summary, our findings show that intravenously delivered IMRCs inhibited both pulmonary inflammation and fibrosis after acute lung injury in vivo. IMRCs significantly improved the survival rate in a dose-dependent manner. Furthermore, the mechanism for amelioration of pulmonary injury may be mediated by the IMRCs' paracrine action rather than their potential to differentiate and replace the damaged alveolar epithelial cells. The IMRCs' functional inhibition of TGF-β1-induced fibrosis could also be part of its mechanism. IMRCs were superior to UCMSCs and pirfenidone in therapeutic efficacy against lung injury and fibrosis. Furthermore, IMRCs showed an excellent safety profile in both mice and monkeys. In light of recent public health crises involving pneumonia, respiratory failure, ALI and ARDS, our pre-clinical results indicate that IMRCs are ready to be carefully considered for human trials in the treatment of lung injury and fibrosis.

Acknowledgements

This work was supported by Beijing Municipal Science & Technology Commission (Z181100003818005 to Qi Zhou), National Key Research and Development Program (2018YFA0108400 and 2017YFA0104403 to Jie Hao, 2017YFA0105001 and 2016YFA0101502 to Liu Wang, 2020YFC0843900 to Qi Zhou, 2020YFC0841900 to Baoyang Hu), the Strategic Priority Research Program of the Chinese Academy of Sciences (XDA16030701 to Liu Wang, XDA16030401 to Wei Li, XDA16040502 to Jie Hao), the National Natural Science Foundation of China (31621004 to Qi Zhou and Wei Li), the Key Research Projects of the Frontier Science of the Chinese Academy of Sciences (QYZDY-SSW-SMC002 to Qi Zhou), and China Postdoctoral Science Foundation (2019M660791 to Liu Wang).

Author contributions

Liu Wang, Baoyang Hu, Huaping Dai and Jie Hao conceived the project and supervised the experiments. These authors contributed equally: Jun Wu, Dingyun Song, Zhongwen Li and Baojie Guo. Jun Wu, Dingyun Song, Zhongwen Li and Baojie Guo wrote the manuscript with help from all the authors. Jun Wu, Dingyun Song, Zhongwen Li, Baojie Guo, Yani Xiao, Wenjing Liu, Lingmin Liang, Chunjing Feng, Tingting Gao, Yanxia Chen, Ying Li, Zai Wang, Jianyan Wen, Shengnan Yang, Peipei Liu, Lei Wang, Yukai Wang, Liang Peng, Hongmei Wang, Tongbiao Zhao, Glyn Nigel Stacey,

Zheng Hu, Guihai Feng, Wei Li, Yan Huo, Ronghua Jin, Ng Shyh-Chang, Qi Zhou, Liu Wang, Baoyang Hu, Huaping Dai and Jie Hao participated in the experiments and data analysis.

Competing interests

The authors declare no conflict of interest.

References

1 Yang, J. & Jia, Z. Cell-based therapy in lung regenerative medicine. *Regenerative medicine research* **2**, 7, doi:10.1186/2050-490x-2-7 (2014).

2 Fan, E., Brodie, D. & Slutsky, A. S. Acute Respiratory Distress Syndrome: Advances in Diagnosis and Treatment. *Jama* **319**, 698-710, doi:10.1001/jama.2017.21907 (2018).

3 Rubenfeld, G. D. *et al.* Incidence and outcomes of acute lung injury. *N Engl J Med* **353**, 1685-1693, doi:10.1056/NEJMoa050333 (2005).

4 Bellani, G. *et al.* Epidemiology, Patterns of Care, and Mortality for Patients With Acute Respiratory Distress Syndrome in Intensive Care Units in 50 Countries. *Jama* **315**, 788-800, doi:10.1001/jama.2016.0291 (2016).

5 Hamacher, J. *et al.* Tumor necrosis factor-alpha and angiostatin are mediators of endothelial cytotoxicity in bronchoalveolar lavages of patients with acute respiratory distress syndrome. *Am J Respir Crit Care Med* **166**, 651-656, doi:10.1164/rccm.2109004 (2002).

6 Raghu, G. *et al.* An official ATS/ERS/JRS/ALAT statement: idiopathic pulmonary fibrosis: evidence-based guidelines for diagnosis and management. *Am J Respir Crit Care Med* **183**, 788-824, doi:10.1164/rccm.2009-040GL (2011).

7 Marshall, R., Bellingan, G. & Laurent, G. The acute respiratory distress syndrome: fibrosis in the fast lane. *Thorax* **53**, 815-817, doi:10.1136/thx.53.10.815 (1998).

8 Dhainaut, J. F., Charpentier, J. & Chiche, J. D. Transforming growth factor-beta: a mediator of cell regulation in acute respiratory distress syndrome. *Critical care medicine* **31**, S258-264, doi:10.1097/01.Ccm.0000057901.92381.75 (2003).

9 King, T. E., Jr. *et al.* A phase 3 trial of pirfenidone in patients with idiopathic pulmonary fibrosis. *N Engl J Med* **370**, 2083-2092, doi:10.1056/NEJMoa1402582 (2014).

10 Yoon, H. Y., Park, S., Kim, D. S. & Song, J. W. Efficacy and safety of nintedanib in advanced idiopathic pulmonary fibrosis. *Respiratory research* **19**, 203, doi:10.1186/s12931-018-0907-8 (2018).

11 Zhou, H., Liu, M. & Lyu, X. [Research progress of mesenchymal stem cells in the treatment of ALI]. *Zhonghua wei zhong bing ji jiu yi xue* **29**, 1039-1042, doi:10.3760/cma.j.issn.2095-4352.2017.11.017 (2017).

12 Serrano-Mollar, A. Cell Therapy in Idiopathic Pulmonary Fibrosis(†). *Med Sci (Basel)* **6**, 64, doi:10.3390/medsci6030064 (2018).

13 Ortiz, L. A. *et al.* Interleukin 1 receptor antagonist mediates the antiinflammatory and antifibrotic effect of mesenchymal stem cells during lung injury. *Proceedings of the*

National Academy of Sciences of the United States of America **104**, 11002-11007, doi:10.1073/pnas.0704421104 (2007).

14 Walter, J., Ware, L. B. & Matthay, M. A. Mesenchymal stem cells: mechanisms of potential therapeutic benefit in ARDS and sepsis. *Lancet Respir Med* **2**, 1016-1026, doi:10.1016/s2213-2600(14)70217-6 (2014).

15 G, W. J. *et al.* Mesenchymal stem (stromal) cells for treatment of ARDS: a phase 1 clinical trial. *The Lancet. Respiratory medicine* **3** (2015).

16 Thomson, J. A. *et al.* Embryonic stem cell lines derived from human blastocysts. *Science (New York, N.Y.)* **282**, 1145-1147, doi:10.1126/science.282.5391.1145 (1998).

17 Barberi, T., Willis, L. M., Socci, N. D. & Studer, L. Derivation of multipotent mesenchymal precursors from human embryonic stem cells. *PLoS medicine* **2**, e161, doi:10.1371/journal.pmed.0020161 (2005).

18 Hwang, N. S. *et al.* In vivo commitment and functional tissue regeneration using human embryonic stem cell-derived mesenchymal cells. *Proceedings of the National Academy of Sciences of the United States of America* **105**, 20641-20646, doi:10.1073/pnas.0809680106 (2008).

19 Vodyanik, M. A. *et al.* A mesoderm-derived precursor for mesenchymal stem and endothelial cells. *Cell stem cell* **7**, 718-729, doi:10.1016/j.stem.2010.11.011 (2010).

20 Gu, Q. *et al.* Accreditation of Biosafe Clinical-Grade Human Embryonic Stem Cells According to Chinese Regulations. *Stem cell reports* **9**, 366-380, doi:10.1016/j.stemcr.2017.04.017 (2017).

21 Pittenger, M. F. *et al.* Multilineage potential of adult human mesenchymal stem cells. *Science (New York, N.Y.)* **284**, 143-147, doi:10.1126/science.284.5411.143 (1999).

22 Pittenger, M. F. *et al.* Mesenchymal stem cell perspective: cell biology to clinical progress. *NPJ Regenerative medicine* **4**, 22, doi:10.1038/s41536-019-0083-6 (2019).

23 Han, X. *et al.* Mapping human pluripotent stem cell differentiation pathways using high throughput single-cell RNA-sequencing. *Genome biology* **19**, 47, doi:10.1186/s13059-018-1426-0 (2018).

24 Kim, D., Langmead, B. & Salzberg, S. L. HISAT: a fast spliced aligner with low memory requirements. *Nature methods* **12**, 357-360, doi:10.1038/nmeth.3317 (2015).

25 Trapnell, C. *et al.* Transcript assembly and quantification by RNA-Seq reveals unannotated transcripts and isoform switching during cell differentiation. *Nature biotechnology* **28**, 511-515, doi:10.1038/nbt.1621 (2010).

26 Huang da, W., Sherman, B. T. & Lempicki, R. A. Systematic and integrative analysis of large gene lists using DAVID bioinformatics resources. *Nature protocols* **4**, 44-57, doi:10.1038/nprot.2008.211 (2009).

27 Subramanian, A. *et al.* Gene set enrichment analysis: a knowledge-based approach for interpreting genome-wide expression profiles. *Proceedings of the National Academy of Sciences of the United States of America* **102**, 15545-15550, doi:10.1073/pnas.0506580102 (2005).

28 Prasad, V. K. *et al.* Efficacy and safety of ex vivo cultured adult human mesenchymal stem cells (Prochymal) in pediatric patients with severe refractory acute graft-versus-host disease in a compassionate use study. *Biology of blood and marrow transplantation : journal of the American Society for Blood and Marrow Transplantation* **17**, 534-541,

792 doi:10.1016/j.bbmt.2010.04.014 (2011).
793 29 Horibata, S., Vo, T. V., Subramanian, V., Thompson, P. R. & Coonrod, S. A. Utilization of
794 the Soft Agar Colony Formation Assay to Identify Inhibitors of Tumorigenicity in Breast
795 Cancer Cells. *Journal of visualized experiments : JoVE*, e52727, doi:10.3791/52727 (2015).
796 30 Zhang, W. *et al.* SIRT6 deficiency results in developmental retardation in cynomolgus
797 monkeys. *Nature* **560**, 661-665, doi:10.1038/s41586-018-0437-z (2018).
798 31 Quinlan, A. R. & Hall, I. M. BEDTools: a flexible suite of utilities for comparing genomic
799 features. *Bioinformatics (Oxford, England)* **26**, 841-842,
800 doi:10.1093/bioinformatics/btq033 (2010).
801 32 Berninger, M. T. *et al.* Fluorescence molecular tomography of DiR-labeled mesenchymal
802 stem cell implants for osteochondral defect repair in rabbit knees. *European radiology* **27**,
803 1105-1113, doi:10.1007/s00330-016-4457-5 (2017).
804 33 Yang, J. *et al.* Tumor tropism of intravenously injected human-induced pluripotent stem
805 cell-derived neural stem cells and their gene therapy application in a metastatic breast
806 cancer model. *Stem cells (Dayton, Ohio)* **30**, 1021-1029, doi:10.1002/stem.1051 (2012).
807 34 Wagers, S., Lundblad, L., Moriya, H. T., Bates, J. H. & Irvin, C. G. Nonlinearity of respiratory
808 mechanics during bronchoconstriction in mice with airway inflammation. *Journal of*
809 *applied physiology (Bethesda, Md. : 1985)* **92**, 1802-1807,
810 doi:10.1152/japplphysiol.00883.2001 (2002).
811 35 Overmyer, K. A., Thonusin, C., Qi, N. R., Burant, C. F. & Evans, C. R. Impact of anesthesia
812 and euthanasia on metabolomics of mammalian tissues: studies in a C57BL/6J mouse
813 model. *PloS one* **10**, e0117232, doi:10.1371/journal.pone.0117232 (2015).
814 36 Lian, Q. *et al.* Derivation of clinically compliant MSCs from CD105+, CD24- differentiated
815 human ESCs. *Stem cells (Dayton, Ohio)* **25**, 425-436, doi:10.1634/stemcells.2006-0420
816 (2007).
817 37 Lee, E. J. *et al.* Novel embryoid body-based method to derive mesenchymal stem cells
818 from human embryonic stem cells. *Tissue engineering. Part A* **16**, 705-715,
819 doi:10.1089/ten.tea.2008.0596 (2010).
820 38 Shi, Y. *et al.* How mesenchymal stem cells interact with tissue immune responses. *Trends*
821 *in immunology* **33**, 136-143, doi:10.1016/j.it.2011.11.004 (2012).
822 39 Milani, S. *et al.* Differential expression of matrix-metalloproteinase-1 and -2 genes in
823 normal and fibrotic human liver. *The American journal of pathology* **144**, 528-537
824 (1994).
825 40 Benyon, R. C., Iredale, J. P., Goddard, S., Winwood, P. J. & Arthur, M. J. Expression of
826 tissue inhibitor of metalloproteinases 1 and 2 is increased in fibrotic human liver.
827 *Gastroenterology* **110**, 821-831, doi:10.1053/gast.1996.v110.pm8608892 (1996).
828 41 Du, C. *et al.* Transplantation of human matrix metalloproteinase-1 gene-modified bone
829 marrow-derived mesenchymal stem cell attenuates CCL4-induced liver fibrosis in rats.
830 *International journal of molecular medicine* **41**, 3175-3184, doi:10.3892/ijmm.2018.3516
831 (2018).
832 42 Sgalla, G. *et al.* Idiopathic pulmonary fibrosis: pathogenesis and management.
833 *Respiratory research* **19**, 32, doi:10.1186/s12931-018-0730-2 (2018).
834 43 Zhu, Y. G., Hao, Q., Monsel, A., Feng, X. M. & Lee, J. W. Adult stem cells for acute lung
835 injury: remaining questions and concerns. *Respirology (Carlton, Vic.)* **18**, 744-756,

836 doi:10.1111/resp.12093 (2013).
837 44 Kanelidis, A. J., Premer, C., Lopez, J., Balkan, W. & Hare, J. M. Route of Delivery Modulates
838 the Efficacy of Mesenchymal Stem Cell Therapy for Myocardial Infarction: A
839 Meta-Analysis of Preclinical Studies and Clinical Trials. *Circulation research* **120**,
840 1139-1150, doi:10.1161/circresaha.116.309819 (2017).
841 45 Weiss, D. J. & Ortiz, L. A. Cell therapy trials for lung diseases: progress and cautions. *Am J*
842 *Respir Crit Care Med* **188**, 123-125, doi:10.1164/rccm.201302-0351ED (2013).

843

844

845

846

847

848 **Figure legends**

Figure 1

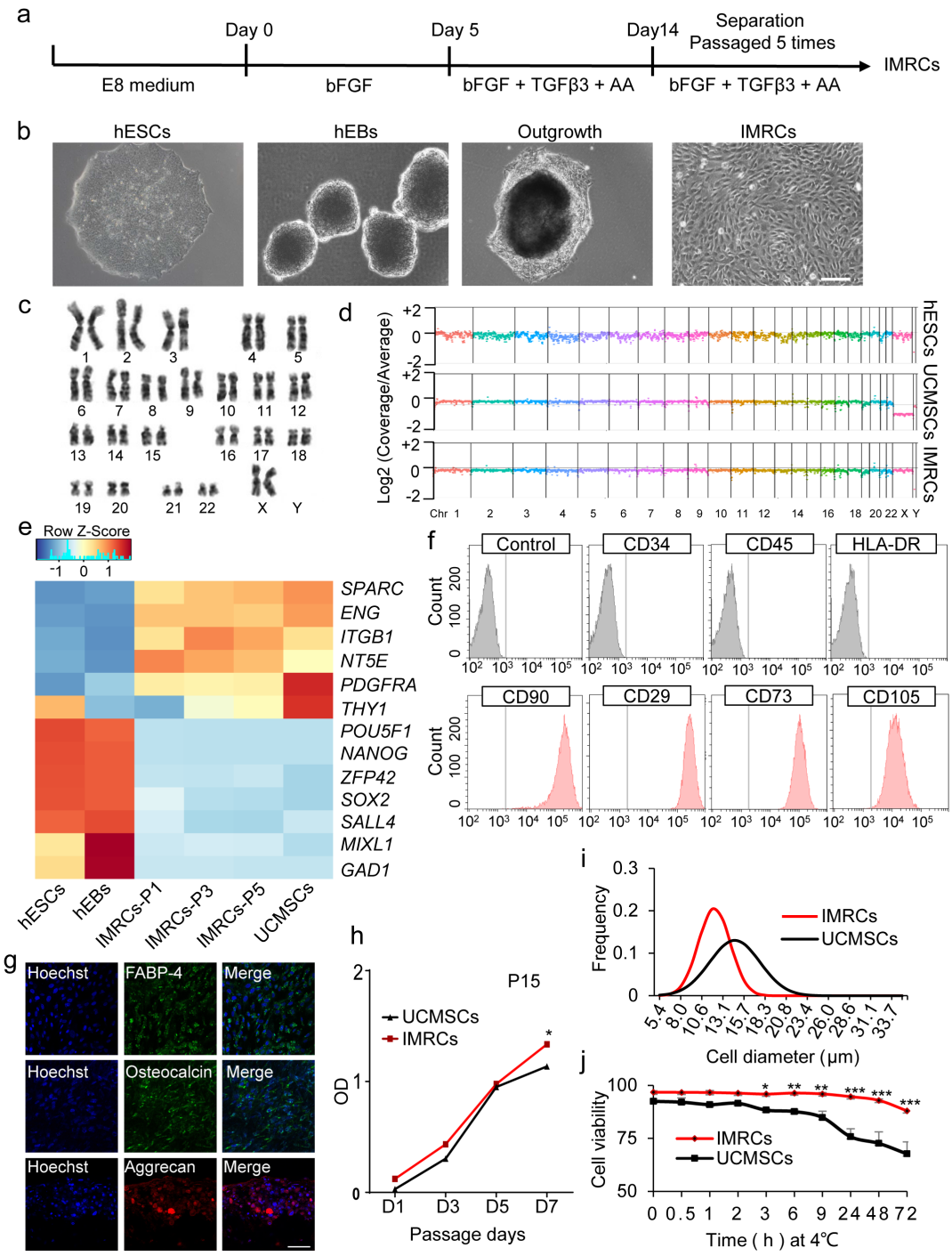

849

850 **Fig. 1 Derivation of immunity- and matrix-regulatory cells (IMRCs) from human embryonic**

851 **stem cells (hESCs).**

852 **a** Different phases of the IMRCs derivation protocol. AA, L-ascorbic acid. **b** Representative

853 morphology of cells at different stages as observed by phase contrast microscopy. hEBs, human

854 embryoid bodies. Scale bars, 100 μm. **c** A representative chromosome spread of normal diploid IMRCs

855 with 22 pairs of autosomes and two X chromosomes. **d** Copy number variation (CNV) analysis by
856 whole genome sequencing for hESCs, primary UCMSCs and IMRCs. UCMSCs, umbilical cord
857 mesenchymal stem cells. **e** Heatmap showing MSC-specific marker and pluripotency marker gene
858 expression changes, from hESCs and hEBs to IMRCs at passages 1-5 (P1-5), and primary UCMSCs. **f**
859 IMRCs' expression of MSC-specific surface markers was determined by flow cytometry. Isotype
860 control antibodies were used as controls for gating. Like MSCs, the IMRCs are $CD34^-$ $CD45^-$
861 $HLA\text{-}DR^-$ $CD90^+$ $CD29^+$ $CD73^+$ $CD105^+$ cells. **g** Representative immunofluorescence staining of
862 IMRCs after they were induced to undergo adipogenic differentiation (FABP-4), osteogenic
863 differentiation (Osteocalcin), and chondrogenic differentiation (Aggrecan). Scale bars, 100 μm. **h**
864 Proliferation curve of IMRCs and UCMSCs at the 15th passage (n=5). **i** Distribution of cell diameters
865 of IMRCs and UCMSCs. **j** Viability of IMRCs and UCMSCs in clinical injection buffer over time at
866 4°C. * $p < 0.05$, ** $p < 0.01$, *** $p < 0.001$; data are represented as the mean ± SEM.

Figure 2

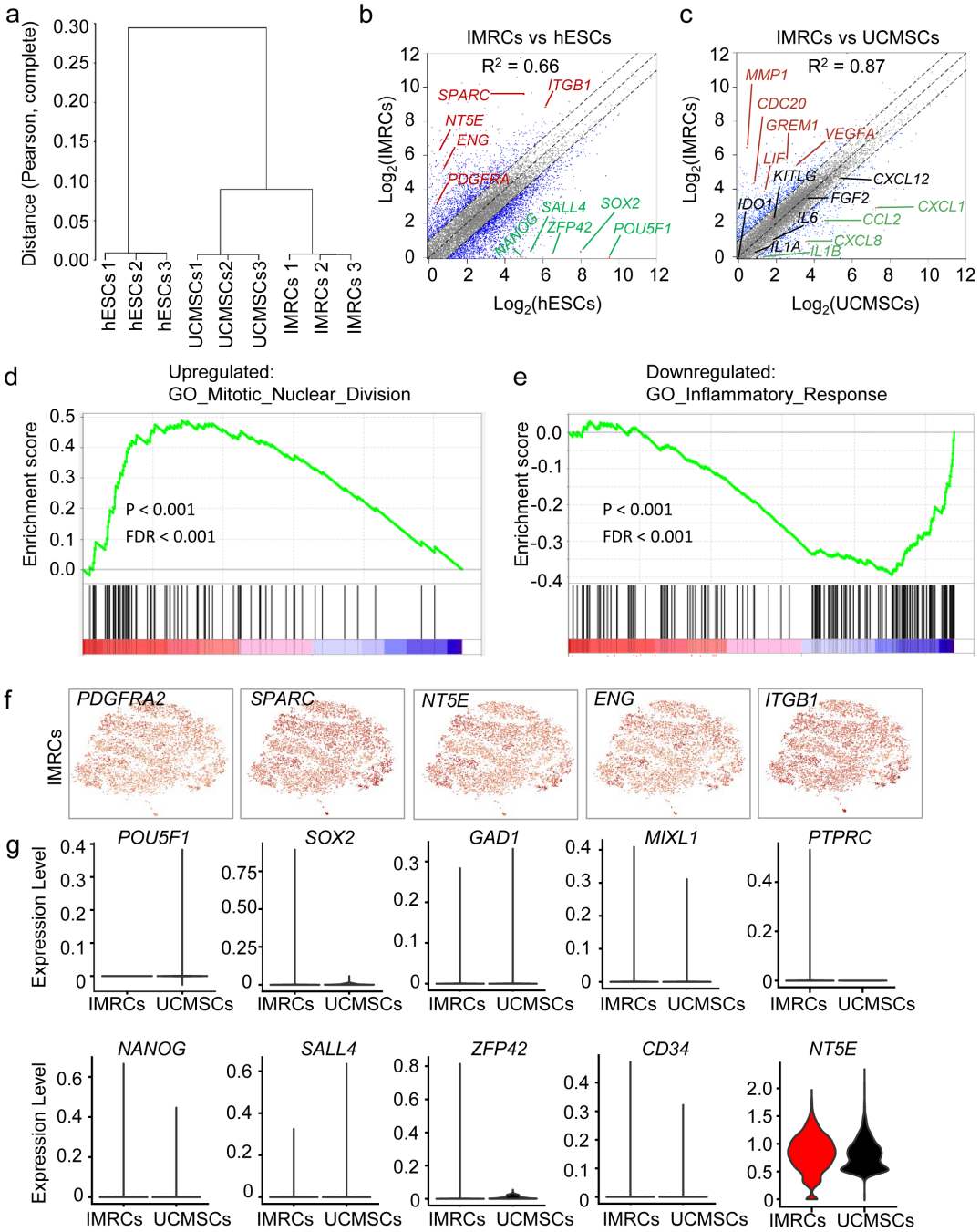

Fig. 2 IMRCs possess unique gene expression characteristics.

a Unsupervised hierarchical clustering analysis based on the Pearson correlation distance between the whole mRNA profile of each cell type. **b** Scatter plot displaying the differentially expressed genes (DEGs) between IMRCs and hESCs. Up-regulated genes are highlighted in red. Down-regulated genes are highlighted in green. Gray dots represent non-DEGs (< 2-fold change). **c** Scatter plot displaying the DEGs between IMRCs and primary UCMSCs. Up-regulated genes are highlighted in red.

Down-regulated genes are highlighted in green. Gray dots represent non-DEGs (< 2-fold change). **d** Gene set enrichment analysis (GSEA) of the top up-regulated gene signature in IMRCs, compared with primary UCMSCs. **e** GSEA of the top down-regulated gene signature in IMRCs, compared with UCMSCs. **f** Heatmaps of specific gene expression amongst single IMRCs groups. **g** Quantification of non-mesenchymal marker gene expression amongst single IMRCs, UCMSCs and hESCs, as measured by single cell RNAseq.

Figure 3

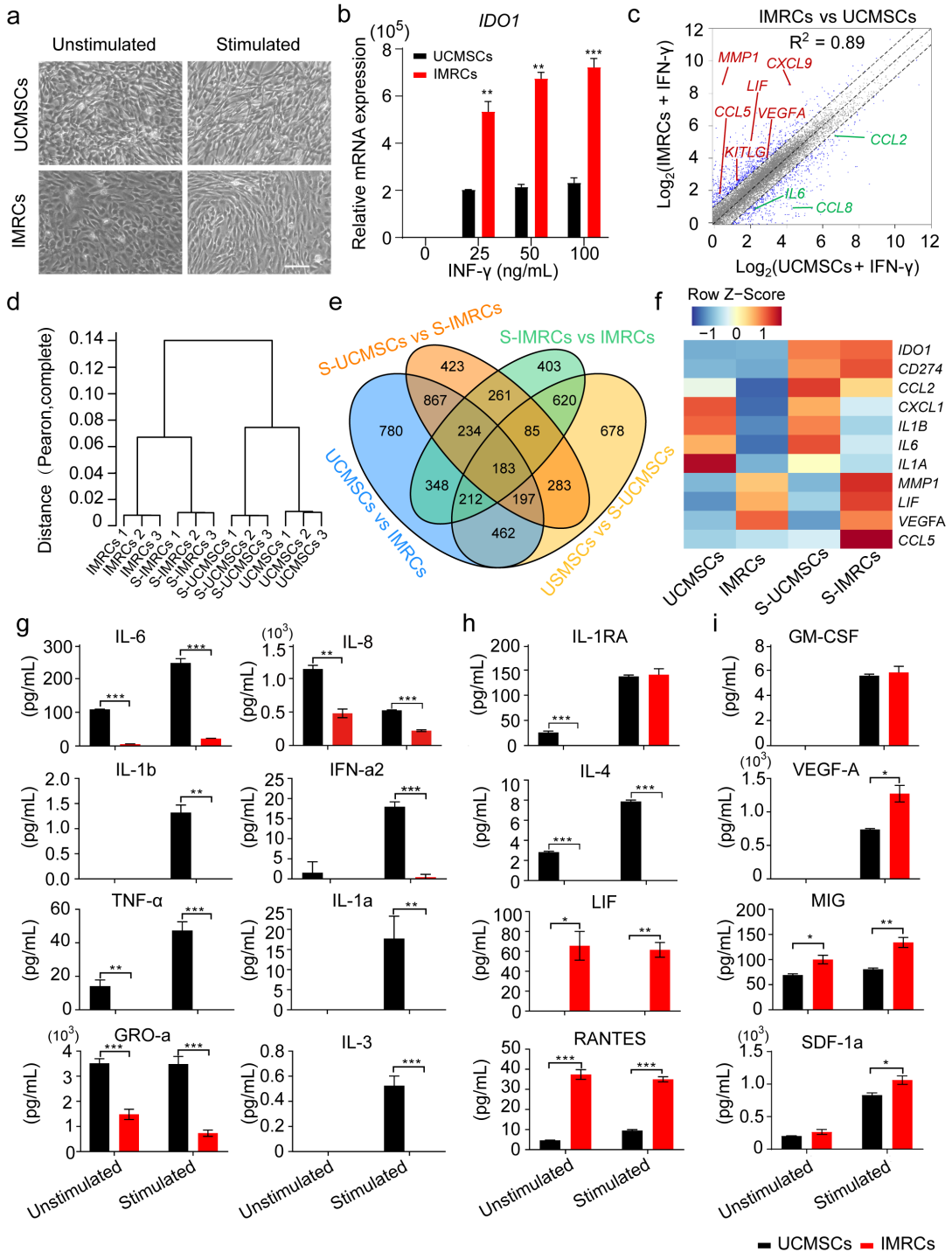

881 **Fig. 3 IMRCs activated by IFN-γ show hyper-immunomodulatory potency.**

882 **a** Morphology of UCMSCs and IMRCs before and after IFN-γ (100 ng/mL) stimulation. **b** Quantitative
883 PCR for *IDO1* mRNA in UCMSCs and IMRCs before and after IFN-γ (0, 25, 50, 100 ng/mL)
884 treatment. *GAPDH* was used for internal normalization. **c** Scatter plot displaying the DEGs between
885 UCMSCs and IMRCs after treatment with 100 ng/mL IFN-γ. Up-regulated genes are highlighted in red.
886 Down-regulated genes are highlighted in green. Gray dots represent non-DEGs (< 2-fold change). **d**
887 Unsupervised hierarchical clustering analysis of UCMSCs and IMRCs, before and after IFN-γ
888 stimulation (S-UCMSCs and S-IMRCs). **e** Venn diagram shows the overlap among UCMSC- and
889 IMRCs -associated genes, before and after IFN-γ stimulation (S). **f** Heatmap illustrating the expression
890 of cytokines in UCMSCs and IMRCs, before and after IFN-γ stimulation (S). **g-i** ELISA analysis of
891 biologically relevant chemokines and cytokines in the secretome of unstimulated or stimulated IMRCs
892 and UCMSCs. Pro-inflammatory (G), immunomodulatory (H), and pro-regenerative (I) cytokines. * p
893 < 0.05, ** $p < 0.01$, *** $p < 0.001$; data are represented as the mean ± SEM. Scale bar, 100 μm.

Figure 4

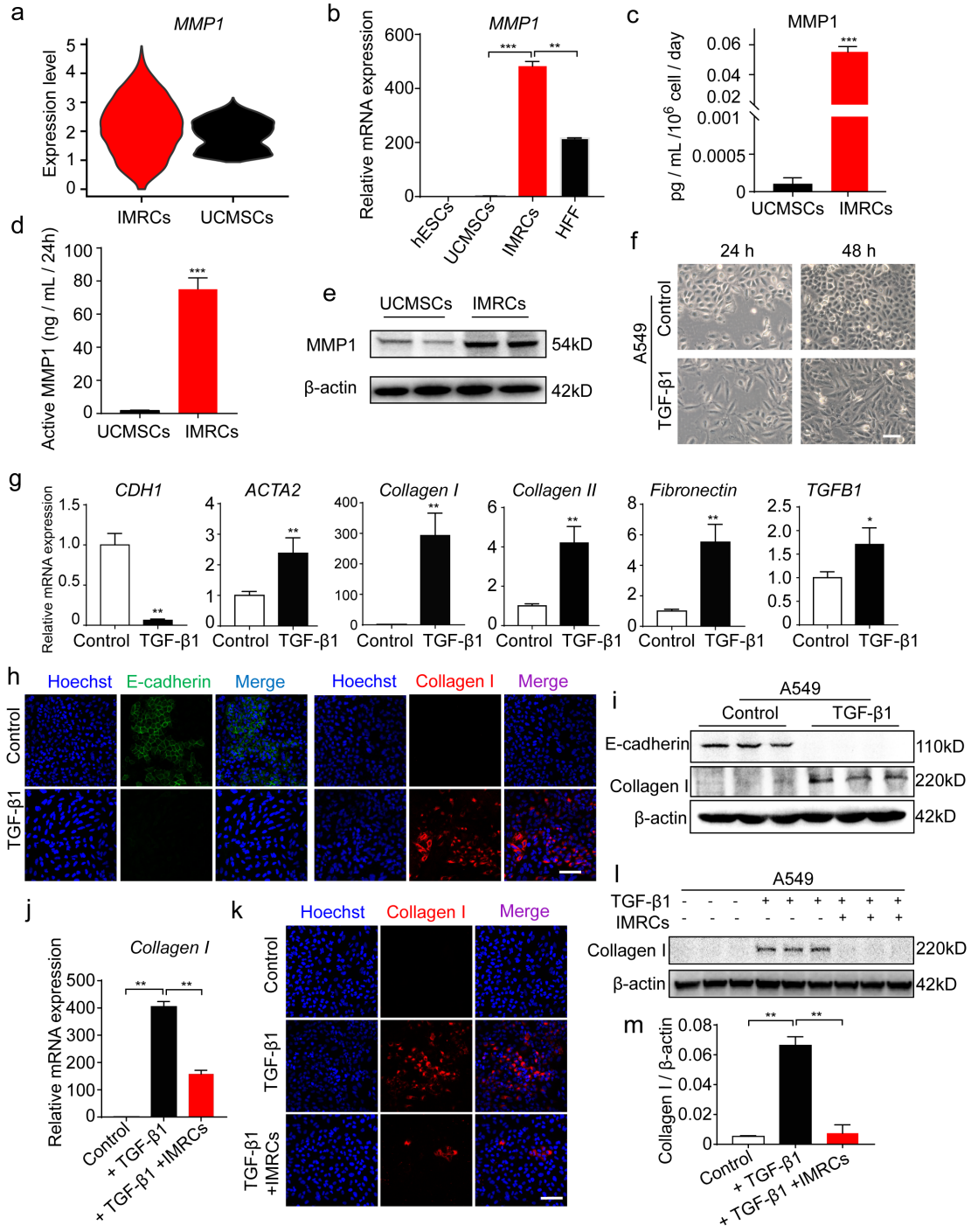

Fig. 4 IMRCs reduce the pro-fibrotic effects of TGF-β1.

a Quantification of *MMP1* gene expression amongst single IMRCs, UCMSCs and hESCs, as measured by single cell RNAseq. **b** Quantitative PCR for *MMP1* mRNA in hESCs, UCMSCs, IMRCs and human foreskin fibroblasts (HFF). **c** ELISA for MMP1 protein in the conditioned media of IMRCs and UCMSCs. **d** MMP1 activity in the conditioned media of IMRCs and UCMSCs. **e** Western blot for MMP1 protein in IMRCs and UCMSCs. β-actin was used as a loading control. **f** Representative

901 morphology of A549 cells, with or without 10 ng/mL TGF-β1 treatment for 48 h. **g** Quantitative PCR
902 for the relative expression of *CDH1*, *ACTA2*, *Collagen I*, *Collagen II, Fibronectin* and *TGFB1* mRNA
903 in A549 cells, with or without TGF-β1 treatment for 48 h. **h** Immunofluorescence staining for
904 E-cadherin and Collagen I expression in A549 cells, with or without 10 ng/mL TGF-β1 treatment for
905 48 h. **i** Western blot for E-cadherin and Collagen I protein expression in A549 cells, with or without 10
906 ng/mL TGF-β1 treatment for 48h. **j** Quantitative PCR for *Collagen I* mRNA in A549 cells, with or
907 without 10 ng/mL TGF-β1 and IMRCs conditioned media treatment for 48 h. **k** Immunofluorescence
908 staining for E-cadherin and Collagen I expression in A549 cells, with or without 10 ng/mL TGF-β1 and
909 IMRCs conditioned media treatment for 48 h. **l** Western blot for E-cadherin and Collagen I protein
910 expression in A549 cells, with or without 10 ng/mL TGF-β1 and IMRCs conditioned media treatment
911 for 48 h. **m** Quantification of the relative Collagen I protein expression levels in **(l)**. * $p < 0.05$, ** $p <$
912 0.01, *** $p < 0.001$; data are represented as the mean ± SEM. Scale bar, 100 μm.

Figure 5

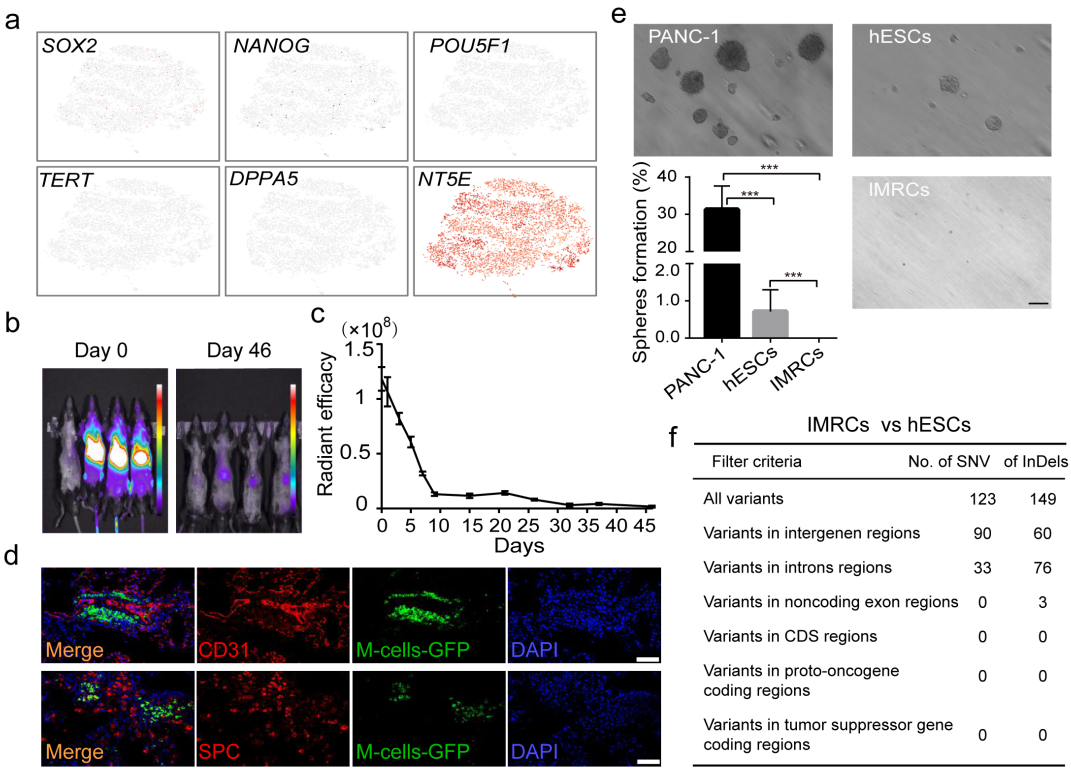

f

IMRCs vs hESCs

Filter criteria	No. of SNV	of InDels
All variants	123	149
Variants in intergenen regions	90	60
Variants in introns regions	33	76
Variants in noncoding exon regions	0	3
Variants in CDS regions	0	0
Variants in proto-oncogene coding regions	0	0
Variants in tumor suppressor gene coding regions	0	0

g Acute toxicity test in cynomolgus monkeys: blood biochemistry (after six months)

Group	ALT (U/L)	AST (U/L)	ALP (U/L)	CK (U/L)	GGT (U/L)	LDH (U/L)	TBIL (μmol/L)	BUN (mmol/L)	CRE (μmol/L)	GLU (mmol/L)	CHO (mmol/L)	TG (mmol/L)
1×10^8	55.00	30.00	165.00	123.00	65.00	497.00	3.00	6.00	58.00	5.00	3.00	1.00
0.26×10^8	73.00	34.00	160.00	164.00	38.54	330.00	3.17	8.00	61.00	4.05	3.83	0.32
0.026×10^8	63.00	49.00	94.00	317.00	51.64	298.00	5.89	7.60	71.00	2.57	2.60	0.32

Group	TP (g/L)	ALB (g/L)	A/G	IgA (g/L)	IgG (g/L)	IgM (g/L)	C3 (g/L)	C4 (g/L)	K^+ (mmol/L)	Na^+ (mmol/L)	Cl^- (mmol/L)
1×10^8	71.00	42.00	1.00	1.00	6.00	1.00	1.00	0.00	3.00	146.00	108.00
0.26×10^8	72.20	42.60	1.44	1.79	7.48	0.76	0.93	0.14	3.62	145.4	98.00
0.026×10^8	78.70	40.90	1.08	2.81	10.81	0.73	0.96	0.09	3.45	146.8	99.80

h Acute toxicity test in cynomolgus monkeys: urinalysis (after six months)

Group	GLU (mmol/L)	PRO (mg/L)	BIL (μmol/L)	URO (μmol/L)	PH	SG	ERY (mg/L)	KET (mmol/L)	NIT	Color
1×10^8	-	-	-	Normal	8.5	<1.005	-	-	-	Light yellow
0.26×10^8	-	+-	-	Normal	8.5	1.015	-	-	-	Yellow
0.026×10^8	-	-	-	Normal	8.0	1.015	-	-	1+	Colorless

Fig. 5 Evaluation of the safety of IMRC transfusion.

a t-SNE projection of single cells and their pluripotency gene expression amongst IMRCs. **b** In vivo imaging of the far red fluorescence in mice after injection of DiR-labeled IMRCs. **c** Quantification of the DiR fluorescent radiance in the whole body over time. **d** Immunofluorescence staining of lung sections for the endothelial marker CD31 and the alveolar epithelial marker SPC, 21 days after injecting GFP-labeled IMRCs. Scale bar, 100 μm. **e** Soft agar colony formation assay for the

920 tumorigenic potential of IMRCs, relative to PANC-1 cancer cells and hESCs. Scale bar, 100 μm. **f**
921 Single nucleotide variants (SNVs) and insertions/deletions (InDels) in the non-repeat regions of the
922 IMRCs genome, relative to hESCs. **g** Blood biochemistry results of cynomolgus monkeys (*Macaca*
923 *fascicularis*) injected with a low (2.6×10^6), medium (2.6×10^7) or high (1×10^8) dose of IMRCs after six
924 months. AST, aspartate aminotransferase; ALT, alanine aminotransferase; ALP, alkaline phosphatase;
925 CK, creatine phosphokinase; GGT, glutamyltransferase; LDH, lactate dehydrogenase; TBIL, total
926 bilirubin; BUN, urea nitrogen; CRE, creatinine; GLU, glucose; CHO, total cholesterol; TG, triglyceride;
927 TP, total protein; ALB, albumin; A/G, albumin/globulin. **h** Urinalysis results of cynomolgus monkeys
928 (*Macaca fascicularis*) injected with a low (2.6×10^6), medium (2.6×10^7) or high (1×10^8) dose of IMRCs
929 after six months. PRO, urine protein; BIL, urine bilirubin; URO, urinary gallbladder; SG, specific
930 gravity; ERY, erythrocyte; KET, ketone; NIT, nitrite. * $p < 0.05$, ** $p < 0.01$, *** $p < 0.001$; data are
931 represented as the mean ± SEM.

Figure 6

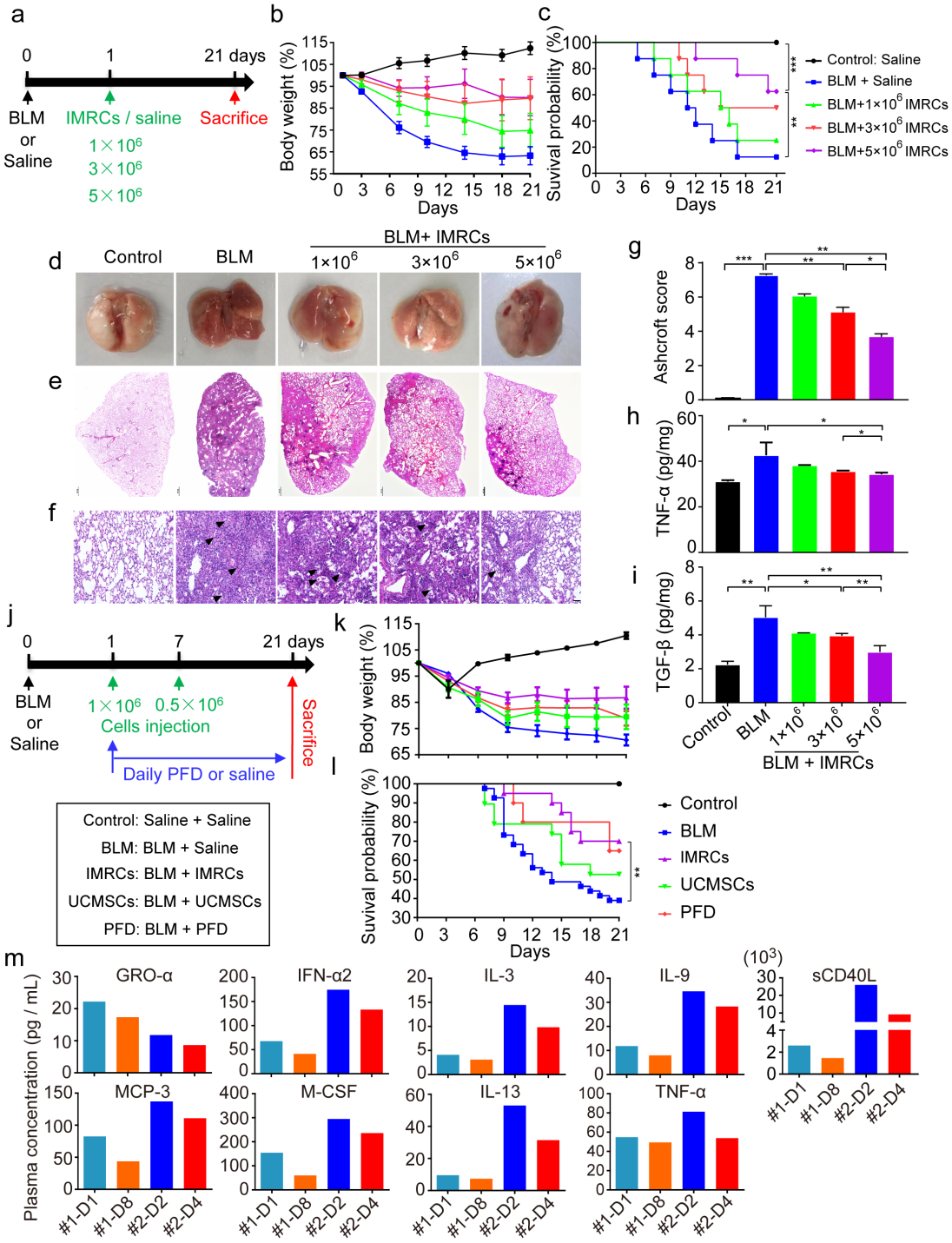

Fig. 6 IMRC transfusion treats lung injury and fibrosis dose-dependently.

a Diagram of the animal experimental protocol for dose escalation. Mice received intratracheal bleomycin (BLM; 2.5 mg/kg body weight) or the same amount of saline at day 0. At day 1, some BLM-injured mice received an intravenous (I.V.) injection of 1×10^6, 3×10^6 or 5×10^6 IMRCs via the caudal vein. A group of BLM-injured mice and normal control mice received the same volume of saline. Mice were randomly grouped (n=8 per group). **b** Relative body weight (%) changes of the mice

939 receiving different interventions. **c** Kaplan-Meier survival curves of the mice receiving different
940 interventions. **d** Representative images of whole lungs from all groups at 21 days post-injury. **e, f**
941 Representative histology of lung sections stained with H&E (Scale bar, 500 μm and 50 μm) at 21 days
942 post-injury. Arrowheads, inflammatory infiltration. **g** Quantitative evaluation of fibrotic changes with
943 the Ashcroft score in lungs of mice receiving different interventions. The Ashcroft scores based on the
944 lung H&E sections. The severity of fibrotic changes in each section was assessed as the mean score of
945 severity in the observed microscopic fields. Six fields per section were analyzed. **h, i** ELISA for the
946 protein levels of TNF-α and TGF-β1 in the lungs of mice receiving different interventions. **j** Diagram
947 of the animal experimental protocol for multiple arm testing. Double I.V. injections of 1×10^6 and
948 0.5×10^6 IMRCs (at days 1 and 7 respectively) were compared side-by-side with double I.V. injections
949 of 1×10^6 and 0.5×10^6 UCMSCs (at days 1 and 7 respectively), vs. daily pirfenidone (PFD) or saline
950 treatments of mice injured with intratracheal bleomycin (BLM; 2.5 mg/kg body weight) at day 0. **k**
951 Relative body weight (%) changes of mice receiving different interventions. **l** Kaplan-Meier survival
952 curves of mice receiving different interventions. **m** ELISA analysis of pro-inflammatory cytokines in
953 the plasma of two ALI patients after intravenous IMRC transfusion. * $p < 0.05$, ** $p < 0.01$, *** $p <$
954 0.001; data are represented as the mean ± SEM.
955